Dynamic relaxation of drifting polymers: A phenomenological approach

Deniz Ertaş and Mehran Kardar
Department of Physics, Massachusetts Institute of Technology, Cambridge, Massachusetts 02139
(Received 18 February 1993)

We study the nonequilibrium dynamic fluctuations of a polymer subject to an external force, moving in a dilute solution at a *uniform* average velocity. Starting from general symmetry arguments, a set of nonlinear equations is proposed to describe the time evolution of the polymer. The dynamic scaling of fluctuations is studied analytically (by renormalization group) and numerically. In most physically relevant cases, the fluctuations are superdiffusive, governed by a swelling exponent $\nu = \frac{1}{2}$ and a dynamic exponent $z = 3$. The polymer exhibits "kinetic" form birefringence as it is stretched by the flow. The crossover to anisotropy is controlled by the scaling variable $y = UN^{1/2}/U^*$, where U is the average velocity, N is the number of monomers, and U^* is a characteristic microscopic velocity that is roughly $10 - 20$ m/s for polystyrene in benzene. Numerical simulations show that strong crossover behavior may produce larger swelling exponents along the force field at intermediate length scales that may potentially give rise to a stretching transition.

PACS number(s): 61.41.+e, 05.40.+j, 64.60.Ht, 78.20.Fm

I. INTRODUCTION AND SUMMARY

The dynamics of polymers in fluids is of much technological interest and has been extensively studied [1,2]. The combination of polymer flexibility, interactions, and hydrodynamics make a first-principles approach to the problem quite difficult. There are, however, a number of phenomenological studies that describe various aspects of this problem [3]. One of the simplest is the Rouse model [4]: The configuration of the polymer at time t is described by a vector $\mathbf{R}(x,t)$, where $x \in [0,N]$ is a continuous variable replacing the discrete monomer index. (See Fig. 1.) Ignoring inertial effects, the relaxation of the polymer in a viscous medium is approximated by

$$\partial_t \mathbf{R}(x,t) = \mu \mathbf{F}(\mathbf{R}(x,t)) = D\partial_x^2 \mathbf{R} + \boldsymbol{\eta}(x,t), \qquad (1.1)$$

where μ is the mobility. The force $\mathbf{F}$ has a contribution from interactions with near neighbors that are treated as springs. (In a coarse-grained formulation the origin of this term is entropic.) Steric and other interactions are ignored. The effect of the medium is represented by the random forces $\boldsymbol{\eta}$ with zero mean. The Rouse model is a linear Langevin equation that is easily solved. It predicts that the mean square radius of gyration $R_g^2 = \langle |\mathbf{R} - \langle \mathbf{R} \rangle|^2 \rangle$ is proportional to the polymer size N and the largest relaxation times scale as the fourth power of the wave number, i.e., in scattering experiments, the half width at half maximum of the scattering amplitude scales as the fourth power of the scattering wave vector $\mathbf{q}$. These results can be summarized as $R_g \sim N^\nu$ and $\Gamma_\mathbf{q} \sim q^z$, where ν and z are called the *swelling* and *dynamic* exponents, respectively. Thus, for the Rouse model, $\nu = 1/2$ and $z = 4$.

The Rouse model ignores hydrodynamic interactions mediated by the fluid. These effects were originally considered by Kirkwood and Risemann [5], and later on by Zimm [6]. The basic idea is that the motion of each monomer modifies the flow field at large distances. Consequently each monomer experiences an additional velocity

$$\delta_H \partial_t \mathbf{R}(x,t) = \frac{1}{8\pi\eta_s} \int dx' \frac{\mathbf{F}(x') r_{xx'}^2 + (\mathbf{F}(x') \cdot \mathbf{r}_{xx'}) \mathbf{r}_{xx'}}{|\mathbf{r}_{xx'}|^3} \approx \int dx' \frac{\gamma}{|x - x'|^\nu} \partial_x^2 \mathbf{R}, \qquad (1.2)$$

where $\mathbf{r}_{xx'} = \mathbf{R}(x) - \mathbf{R}(x')$, and the final approximation is obtained by replacing the actual distance between two monomers by their average value. The modified equation is still linear in $\mathbf{R}$ and easily solved. The main result is the speeding up of the relaxation dynamics as the exponent z changes from 4 to 3. Most experiments on polymer dynamics indeed measure exponents close to 3 [7]. Rouse dynamics is still important in other circumstances, such as the diffusion of a polymer in a solid matrix, stress and viscoelasticity in concentrated polymer solutions, and is also applicable to relaxation times in Monte Carlo simulations [1].

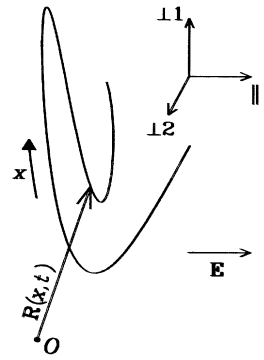

FIG. 1. Configurations of the polymer at time t are described by $\mathbf{R}(x,t)$, where x labels the monomer index.

There are also many studies of the morphology of polymers in shear flows. The approach is usually to follow the evolution of a probability distribution for the shape of the polymer under the combined action of shear and elastic forces [8]. Under some circumstances the shear force may cause a coil-to-rod transition [9]. In this paper we consider the dynamics of a polymer drifting through the fluid *at a constant velocity* U, due to a uniform external force $\mathbf{E}$, and in the absence of any external velocity gradients. Specific examples include *sedimentation* of polymers, in which case $\mathbf{E}$ is the acceleration due to gravity $\mathbf{g}$ and *gel electrophoresis* [10] where $\mathbf{E}$ is the electric field.

At first sight it may appear that there should be no difference in the relaxation dynamics of a polymer at rest and one moving at a uniform velocity. This conclusion is in fact not correct due to the interactions with the surrounding fluid. For example, the drift velocity of a rod pulled through a viscous fluid depends on its orientation relative to the force [3]. (In principle the force acting on a linear object can be calculated from the equations of "slender body theory" [11].) Therefore, the motion of a monomer, more accurately modeled as a cylindrical rod along the chain rather than a spherical bead, in general depends on its orientation relative to the driving force. Thus, as $\mathbf{E}$ (and consequently U) is increased, there should be a crossover to a regime where the anisotropy is no longer negligible. The scale of this crossover can be estimated from dimensional analysis alone: For physical quantities that involve the whole polymer, like form birefringence, the natural length scale is the radius of gyration, $R_g = b_0 N^\nu$. The parameter D appearing in Eq. (1.1) has dimensions of (length)^2/(time). We can thus construct a dimensionless parameter $y = UR_g/D = UN^\nu/U^*$, where $U^* = D/b_0 = b_0/\tau_0$ is a characteristic velocity. Here b_0 and τ_0 are microscopic length and time scales for the monomers. For *both* the Rouse and Zimm models, this quantity is given roughly by $U^* \approx kT/(\pi\eta_s b_0^2)$. For a dilute solution of polystyrene in benzene (after Adam and Delsanti [7]), $U^* \approx 10$ m/s. For a polymer with molecular weight $M_W = 10^6$, $y \approx 1$ when $U \approx 4$ cm/s. Another calculation, using the relaxation time data from Farrell *et al.* [7] yields $U^* \approx 20$ m/s, about the same order of magnitude. (Not surprisingly, y is proportional to the Reynolds number, $\mathrm{Re} = UR_g/\eta_s$, corresponding to the polymer size, i.e., the same variable also controls the crossover to hydrodynamic instabilities [12].) Yet another scaling argument considers energetics: The energy scale associated with monomer orientation is roughly Eb_0, where b_0 is the monomer length. This should be compared to the energy of thermal fluctuations, which scales as kT. For a polymer with N monomers, the thermal fluctuations add up as independent random variables unlike orientational energies. Thus comparing these two total-energy scales, we once again obtain the scaling variable

$$y \approx \frac{NEb_0}{N^{1/2}kT} \approx \frac{UN^{1/2}}{kT/6\pi\eta_s b_0^2} \approx \frac{UN^{1/2}}{U^*}, \tag{1.3}$$

where the Rouse mobility relation $E = 6\pi\eta_s b_0 U$ was used in the second identity.

We are primarily interested in understanding the static and dynamical scaling properties of the nonlinear and anisotropic regime for $U \gtrsim U^*$. A first-principles approach to the problem is quite difficult due to the complexity of the system and the nonequilibrium nature of the problem. We shall instead take a phenomenological route and construct the equations of motion based on symmetry considerations. Such an approach has been successful in describing other nonequilibrium problems [13].

As in the case of the Rouse model, we shall neglect inertial effects and write the velocity of a point on the polymer (Fig. 1) as

$$\partial_t \mathbf{R}(x,t) = \mu \mathbf{F}(\partial_x \mathbf{R}(x,t), \partial_x^2 \mathbf{R}(x,t), \ldots; \mathbf{e}(x,t)). \tag{1.4}$$

We shall restrict ourselves to forces $\mathbf{F}$ that are *local*, but that can be expanded in powers of gradients of $\mathbf{R}$. (Due to the translational symmetry $\mathbf{R} \mapsto \mathbf{R} + \mathbf{c}$, $\mathbf{R}$ cannot appear in the equations of motion.) The effects of steric interactions, and nonlocal hydrodynamic forces as in Eq. (1.2), will be discussed later. Nonequilibrium effects enter through the external force $\mathbf{e} = \mathbf{E} + \delta\mathbf{e}$, with a *nonzero average* value of $\mathbf{E}$, and fluctuations $\delta\mathbf{e}(x,t)$ due to thermal stochasticity and other sources of disorder in the solvent. We assume that any barriers to motion in the medium are isotropic, and sufficiently weak that the polymer reaches a *steady state* where its "center of mass," $\mathbf{R}_0(t)$, is *depinned* and moves with a uniform velocity. The leading terms in the expansion of Eq. (1.4) yield (see Appendix A) the evolution of relative monomer positions, $\mathbf{r}(x,t) = \mathbf{R}(x,t) - \mathbf{R}_0(t)$, as

$$\partial_t r_\parallel = D_\parallel \partial_x^2 r_\parallel + \frac{\lambda_\parallel}{2}(\partial_x r_\parallel)^2 + \frac{\lambda_\times}{2}\sum_{i=1}^{n}(\partial_x r_{\perp i})^2 + \eta_\parallel(x,t), \tag{1.5a}$$

$$\partial_t r_{\perp i} = D_\perp \partial_x^2 r_{\perp i} + \lambda_\perp \partial_x r_\parallel \partial_x r_{\perp i} + \eta_{\perp i}(x,t). \tag{1.5b}$$

In the above equation, and henceforth, we shall use the symbols $\parallel$ and $\{\perp i\}$ to indicate the components parallel (longitudinal) or perpendicular (transverse) to the force field. For the general case of a polymer embedded in a d-dimensional space, there are $n = d - 1$ transverse coordinates $\{\perp i\}$. The noise η_α has zero mean, but unlike thermal noise need not be isotropic, and its second cumulants [14] satisfy

$$\langle \eta_\parallel(x,t)\eta_\parallel(x',t')\rangle = 2T_\parallel \delta(x-x')\delta(t-t'), \tag{1.6a}$$

$$\langle \eta_{\perp i}(x,t)\eta_{\perp j}(x',t')\rangle = 2T_\perp \delta_{i,j}\delta(x-x')\delta(t-t'). \tag{1.6b}$$

The equations of motion (1.5) and (1.6) are already "coarse grained" in both space and time, i.e., faster modes associated with the motion of the fluid around the polymer have been integrated out. The resulting noise correlations may have long-range correlations; this possibility will be discussed later. The nonlinear coefficients $\{\lambda_\parallel, \lambda_\times, \lambda_\perp\}$ must vanish in equilibrium due to invariance of the equations under $\mathbf{r} \mapsto -\mathbf{r}$. As shown in Appendix A, the external field breaks this symmetry, and hence these coefficients are proportional to E for small fields. One source of such nonlinearity is the

hydrodynamic interactions of the polymer with the solvent. They can be estimated by starting from the Rouse model, but regarding each monomer as a slender rod [11], oriented along $\partial_x \mathbf{r}$, rather than a spherical bead. The mobility of each rod is then a function of its *orientation* [1], and a brief calculation of the resulting nonlinear effects is given in Appendix B. The results show that to lowest order in the applied field, all three nonlinear coefficients are positive. However, symmetry considerations alone do not restrict their signs. Without loss of generality we shall assume that $\lambda_{\parallel}$ is positive and finite (its sign can be changed by $r_{\parallel} \to -r_{\parallel}$), and focus on the behavior of the polymer as a function of the ratios $\lambda_{\perp}/\lambda_{\parallel}$ and $\lambda_{\times}/\lambda_{\parallel}$, as in Fig. 2. (The vertical axis is actually chosen as $\lambda_{\times} T_{\perp} D_{\parallel}/\lambda_{\parallel} T_{\parallel} D_{\perp}$ for the convenience of demonstrating renormalization-group trajectories.)

In the absence of transverse fluctuations, i.e., $n = 0$, Eqs. (1.5) reduce to the Kardar, Parisi, and Zhang (KPZ) equation [15] that describes a growing surface in two dimensions. Thus the transverse components can also be interpreted as scalar fields that couple locally to the profile of the growing interface [16]. For example, the special case of $\lambda_{\perp} = 0$ corresponds to n diffusive scalar fields coupled nonlinearly to an order parameter $r_{\parallel}$. The results for the special case $n = 1$ were presented in an earlier work [17], in the context of the motion of a (directed) vortex line. Here, we shall investigate the more general problem with the emphasis on $n = 2$ describing polymers in three-dimensional space.

The noise-averaged correlation functions of Eqs. (1.5) satisfy the dynamic scaling form

$$\langle [r_\alpha(x,t) - r_\alpha(x',t')]^2 \rangle = |x - x'|^{2\nu_\alpha} f_\alpha \left(\frac{|x - x'|^{\zeta_\alpha}}{|t - t'|} \right), \tag{1.7}$$

where f_α are scaling functions, ν_α and $z_\alpha = \zeta_\alpha/\nu_\alpha$ are the *swelling* and *dynamic* exponents, respectively. (The exponent ζ is introduced for convenience in the renormalization-group (RG) procedure. The index α refers to either the longitudinal or any of the n transverse components.) In the absence of nonlinearities, the independent diffusion equations can be solved *exactly* to give $\nu_{\parallel} = \nu_{\perp i} = 1/2$ and $z_{\parallel} = z_{\perp i} = 4$. A RG treatment, perturbative in the nonlinearities, indicates that all the nonlinear terms in Eqs. (1.5) are relevant and may modify the exponents in Eq. (1.7). Recent studies of related stochastic equations [18,19] indicate that interesting dynamic phase diagrams may emerge from the competition between nonlinearities. Surprisingly, in most cases the nonlinearities reduce the exponent z to 3, the value obtained from the Zimm model in Eq. (1.2). (This is a coincidence, but indicates that the nonlinearities can mimic some of the effects of hydrodynamic interactions.) Furthermore, the model parameters in Eqs. (1.5) and (1.6) become anisotropic in general under RG, which implies the existence of a kinetically induced form birefringence *even in the absence of an external velocity gradient.* This change in scaling from Rouse dynamics is controlled by the dimensionless parameters $\lambda^2 T/D^3$, not surprisingly scaling as $(U\ell^{1/2}/U^*)^2$, where ℓ is the coarse-grained length scale. Thus, all the effects discussed in subsequent sections become important when $y \geq 1$.

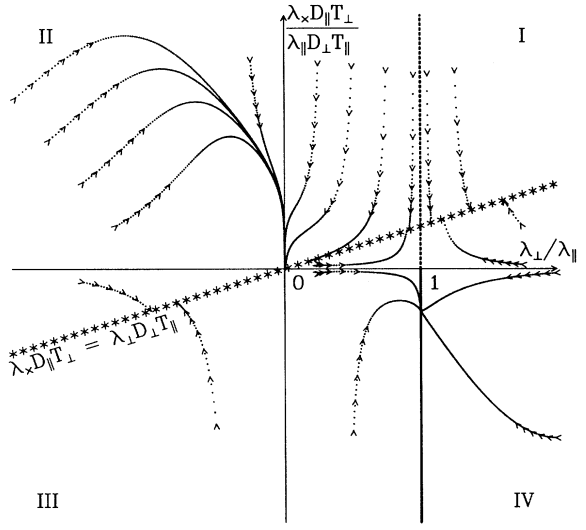

FIG. 2. A projection of the RG flows in Eqs. (3.7) for $n = 1$. The quadrants mentioned in the text are shown in roman numerals. The conditions necessary for Galilean invariance, Cole-Hopf transformation, and fluctuation-dissipation, are indicated by dotted, bold, and starred lines, respectively. The projected RG flows are constrained by these lines.

In order to justify the applicability of Eqs. (1.5) to real polymers, we have to address the importance of terms left out of the local description. Since the Zimm model is the correct starting point for polymers at rest, paramount among these is the long-range hydrodynamic interactions appearing in Eq. (1.2). However, while the hydrodynamic interactions are strongly relevant at the Rouse fixed point, they are only marginal at the nonlinear fixed point of Eqs. (1.5). (This is because z is already 3 at this fixed point.) In fact even self-avoiding interactions, usually left out of the Zimm treatment, are also marginal, indicating the robustness of this behavior. The remaining source of difficulty is a nonlinear *and* nonlocal term described in Sec. V. The magnitude of this term is likely to be small, but if it becomes relevant, it could signal yet another scaling regime, possibly one in which the polymer completely unravels and becomes stretched.

The rest of the paper is organized as follows. In Sec. II we address a number of nonperturbative properties of Eqs. (1.5), that will be helpful in interpreting the RG recursion relations (3.7). One such property is a *Galilean invariance* (GI) that, for the case $\lambda_{\parallel} = \lambda_{\perp}$, implies an exact exponent identity $\nu_{\parallel} + \nu_{\parallel} z_{\parallel} = 2$. This identity holds as long as the noise has only short-time correlations. The *Cole-Hopf* (CH) *transformation* is an important method for the exact study of solutions to the one-component nonlinear diffusion equation [20]. We present a generalization that extends the applicability of this method to arbitrary n. This enables an analytic solution to the *de-*

terministic equation and is a useful tool in studying the full stochastic equation by path integral methods. In particular for $n = 1$, the exact exponents $z_{\|} = 3, \nu_{\|} = 1/2$ are obtained. Finally, we investigate special cases where a *fluctuation-dissipation* (FD) *theorem* can be written for the system, which leads to the exact exponent values $\nu_{\|} = \nu_{\perp} = 1/2$. The regions in parameter space, where these properties are applicable, are indicated in Fig. 2.

In Sec. III, we present a one-loop dynamical RG calculation, perturbatively in the nonlinear couplings, which determines the scaling exponents ν_α and ζ_α. At the point $\lambda_{\|} > 0$, $\lambda_{\perp} = \lambda_{\times} = 0$ the equations for $r_{\|}$ and $r_{\perp i}$ decouple, and $\zeta_{\perp} = 2$ while $\zeta_{\|} = 3/2$. However, in general we expect $\zeta_{\|} = \zeta_{\perp} = \zeta$ unless the effective $\lambda_{\perp}$ is zero. For example, at the intersection of the subspaces with GI and FD (see Sec. II) the exact exponents $\nu_{\|} = \nu_{\perp} = 1/2$ and $\zeta_{\|} = \zeta_{\perp} = 3/2$ are obtained by utilizing the exponent identities. To construct the RG equations, we use only one value of ζ and check for consistency by requiring that $\lambda_{\perp}$ renormalizes to a finite nonzero value. (The perturbative RG treatment breaks down when $\zeta_{\perp} \neq \zeta_{\|}$, this limits the usefulness of this method.) Under a change of scale, $x \to e^{\ell}x$, $t \to e^{\zeta\ell}t$, $r_{\|} \to e^{\nu_{\|}\ell}r_{\|}$, and $r_{\perp i} \to e^{\nu_{\perp}\ell}r_{\perp i}$, the renormalization of the parameters in Eqs. (1.5), computed to one-loop order by standard methods of dynamic RG [21,22], is given in Eqs. (3.7). The projections of the RG flows on the two-parameter subspace of Fig. 2 are also indicated in this diagram. The resulting exponents are discussed below in conjunction with those of numerical integrations.

Section IV describes details of the direct numerical integrations of Eqs. (1.5), used to determine the exponents numerically. The scaling behavior in the various regions, obtained by combining nonperturbative, RG, and numerical results, is as follows.

$1 \leq n < 4$. In this case, the recursion relations give rise to the flow in parameter space like the one shown in Fig. 2. When all three nonlinear terms have *the same sign* (quadrant I in Fig. 2), the RG flows terminate on the fixed line where FD conditions apply, and the exponents assume fixed-point values $\nu_\alpha = 1/2$ and $\zeta_\alpha = 3/2$ ($z_\alpha = 3$). The equilibrium polymer shape in this case is an ellipsoid, with an aspect ratio that depends on $D_{\|}T_{\perp}/D_{\perp}T_{\|}$ which varies continuously along the fixed FD line. In three dimensions ($n = 2$), starting from the $\{\lambda\}$ values calculated in Appendix B, we followed the RG flow to determine the fixed-point anisotropy, obtaining $\langle r_{\|}^2\rangle/\langle r_{\perp}^2\rangle \approx 6$. However, the fixed-point value is reached only for very long polymers ($\approx 10^7$ persistence lengths) unless the external force is large, in which case the assumptions in Appendix B are inappropriate. When $\lambda_{\perp} = 0$, transverse and longitudinal components decouple, resulting in a simple diffusion equation for $r_{\perp i}$, with $\zeta_{\perp} = 2$. Since $\lambda_{\times} \neq 0$, the transverse components act as a strongly correlated (both in space and time) noise [21] on the longitudinal component. There is no finite scale-invariant fixed point and the RG is inconclusive. A naive application of the results in Ref. [21], treating this coupling as a noise correlated in space only, gives $\nu_{\|} = 2/3$ and $\zeta_{\|} = 4/3$ ($z_{\|} = 2$). Numerical results give an even larger swelling exponent $\nu_{\|}$ (see Table I), which seems to increase with system size, suggesting a change in the scaling properties of the system [23]. A polymer with swelling exponents $\nu_{\|} > \nu_{\perp}$ is elongated and cigar shaped. On the other hand, when $\lambda_{\times} = 0$, the longitudinal displacement satisfies the KPZ equation, i.e., $\nu_{\|} = 1/2$, $\zeta_{\|} = 3/2$ ($z_{\|} = 3$). Its coupling to the transverse components, however, changes the scaling exponents to $\nu_{\perp} = 0.75$, $\zeta_{\perp} = 3/2$ ($z_{\perp} = 2$). With swelling exponents $\nu_{\perp} > \nu_{\|}$, the polymer assumes a pancake shape. This increased value of $\nu_{\perp}$ is verified by the numerical results as well, as seen in Table I. In the light of these results, different scaling behaviors are anticipated when the nonlinearities have *different relative signs*. The recursion relations (3.7) indicate that the flows do not terminate at a finite fixed point in quadrants II and IV of Fig. 2. It is possible that there is no steady state in this region, and the numerical integration procedure indeed suffers instabilities caused by discretization. The exponents quoted in this regime are obtained from examining the correlation functions over short times before the instabilities take over. As such they are not reliable, at most reflecting the qualitative changes in these regions of parameter space. For the case $\lambda_{\perp} > 0$ and $\lambda_{\times} < 0$ (quadrant IV), the RG flows converge to a subspace where the CH transformation, discussed in Sec. II, is applicable, suggesting $\nu_{\|} = 1/2$, $\zeta_{\|} = 3/2$. Since $\lambda_{\perp}$

TABLE I. Numerical estimates of the scaling exponents, for various values of model parameters for $n = 1$. In all cases, $D_{\|} = D_{\perp} = 1$ and $T_{\|} = T_{\perp} = 0.01$, unless indicated otherwise. Typical error bars are ± 0.05 for ν, ± 0.1 for z. Entries in parentheses are theoretical results. Exact values are given in fractional form.

$\lambda_{\|}$	$\lambda_{\times}$	$\lambda_{\perp}$	$\nu_{\|}$	$z_{\|}$	$\nu_{\perp}$	$z_{\perp}$
20	20	20	0.48	3.0	0.48	3.0
			(1/2)	(3)	(1/2)	(3)
20	20	2.5	0.75	1.7	0.50	3.7
20	5	25	0.51	3.4	0.56	2.9
5	5	-5	0.83	unstable	0.44	3.6
			(No fixed point for finite ν, ζ)			
20	-20	-20	0.50	3.1	0.50	2.9
			(1/2)	(3)	(1/2)	(3)
5	-5	5	0.52	3.3	0.57	3.4
			(1/2)	(3)	(Strong coupling)	
20	0	20	0.49	3.1	0.72	2.2
			(1/2)	(3)	(0.75)	(2)
20	0	-20	0.48	3.0	0.65	3.1
			(1/2)	(3)	($\zeta_{\perp} > \zeta_{\|}$)	
20	20	0	0.84	1.4	0.50	4.0
			($\zeta_{\|} < \zeta_{\perp}$)		(1/2)	(4)
20	-20	0	0.55	2.9	0.51	4.0
			($\zeta_{\|} < \zeta_{\perp}$)		(1/2)	(4)

TABLE II. Numerical estimates of scaling exponents for the parameter values $D_\parallel = D_\perp = 1$, $\lambda_\parallel = \lambda_\times = \lambda_\perp = 20$, and $T_\parallel = T_\perp = 0.01$, for different number of transverse components n.

n	$\nu_\parallel$	$z_\parallel$	$\zeta_\parallel$	$\nu_\perp$	$z_\perp$	$\zeta_\perp$
2	0.49	3.1	1.53	0.48	3.1	1.50
3	0.54	2.8	1.52	0.49	3.1	1.55
4	0.50	2.6	1.33	0.50	3.3	1.64
5	0.51	2.8	1.42	0.50	3.2	1.62
6	0.49	2.6	1.27	0.50	3.2	1.61

remains finite, we expect $\zeta_\perp = \zeta_\parallel = 3/2$, but there is no information on $\nu_\perp$. For the case $\lambda_\perp < 0$ and $\lambda_\times > 0$, none of the methods employed give a definite result. RG exponents diverge as $\ell \to \infty$, and there are no applicable nonperturbative arguments. Numerical results show the trend towards a large $\nu_\parallel$, but fail to give a definite result due to instabilities in the discretized integration. It is possible that higher-order terms in the equation of motion are necessary to determine the correct behavior of the system. When both $\lambda_\perp$ and $\lambda_\times$ have signs opposite to that of $\lambda_\parallel$, the system settles back to the scaling behavior $\nu_\alpha = 1/2$, $\zeta_\alpha = 3/2$, the RG flows terminating at the FD fixed line.

$n \geq 4$. The perturbative RG now breaks down as the expansion parameters diverge. (Specifically, $D_\perp/D_\parallel \to 0$ in quadrant I.) However, nonperturbative, i.e., exact, results still hold. In order to see the effect of increasing n, we have numerically integrated the system at the point where both the GI and FD conditions are satisfied. The measured exponents for up to $n = 6$ are given in Table II. The exact swelling exponents $\nu_\parallel = \nu_\perp = 1/2$ are recovered, in compliance with the fluctuation-dissipation theorem (FDT) condition, but the dynamical exponents seem to depart from $\zeta = 3/2$. This behavior does not conflict with the GI condition, which implies $d(\ln \lambda_\parallel)/d\ell = \nu_\parallel + \zeta - 2$, since it is possible that $\nu_\parallel + \zeta_\parallel < 2$ and $\lambda_\parallel$ is *irrelevant.* Thus there is a possibility that for large n, the system goes to a regime where the dynamical exponents are different. This region therefore needs further attention and analysis.

Finally, in Sec. V, we discuss several straightforward generalizations of the model to directed flux lines and to drifting membranes. We also examine the relevance of long-range correlated noise, hydrodynamic interactions, and steric constraints. Surprisingly, we find that both effects are much less important in the presence of nonlinearities.

II. NONPERTURBATIVE PROPERTIES

For special choices of their parameters, Eqs. (1.5) satisfy some important properties, which are addressed in this section.

A. Galilean invariance

For $\lambda_\parallel = \lambda_\perp$, Eqs. (1.5) are unchanged by the infinitesimal transformation

$$x' = x - \lambda_\parallel \epsilon t \ , \ t' = t \ , \qquad (2.1)$$
$$r'_\parallel = r_\parallel + \epsilon x \ , \ r'_{\perp i} = r_{\perp i} \quad (i = 1, n).$$

This result can be established by noting that under the change of coordinates, the derivatives transform as

$$\partial_x = \partial_{x'} \ , \qquad (2.2)$$
$$\partial_t = \partial_{t'} - \epsilon\lambda_\parallel \partial_{x'} \ .$$

In particular, in terms of the transformed distortions, $\partial_x r_\parallel = (\partial_{x'} r'_\parallel - \epsilon)$, while $\partial_x r_{\perp i} = \partial_{x'} r_{\perp i}$. Using this information we can rewrite Eqs. (1.5) as

$$(\partial_{t'} - \epsilon\lambda_\parallel \partial_{x'})(r'_\parallel - \epsilon x)$$
$$= D_\parallel \partial^2_{x'} r'_\parallel + \frac{\lambda_\parallel}{2}(\partial_{x'} r'_\parallel - \epsilon)^2$$
$$+ \sum_{i=1}^{n} \frac{\lambda_\times}{2}(\partial_{x'} r'_{\perp i})^2 + \eta_\parallel(x' - \lambda_\parallel \epsilon t', t'), \qquad (2.3)$$

$$(\partial_{t'} - \epsilon\lambda_\parallel \partial_{x'})(r'_{\perp i}) = D_\perp \partial^2_{x'} r'_{\perp i} + \lambda_\perp(\partial_{x'} r'_\parallel - \epsilon)\partial_{x'} r'_{\perp i}$$
$$+ \eta_\perp(x' - \lambda_\parallel \epsilon t', t') \ . \qquad (2.4)$$

Keeping terms to order of ϵ, we see that the deterministic part of the above equations becomes identical to Eqs. (1.5) for $\lambda_\parallel = \lambda_\perp$. The transformed noise is evaluated at a different point, but it is easy to see that its correlations still satisfy Eqs. (1.6). In fact this invariance holds even for noise that has spatial (but not temporal) correlations [21]. The significance of this invariance lies in the fact that $\lambda_\parallel$ appears both in the transformation and the equations of motion (1.5). Consequently it cannot be changed by any rescaling of the equation that preserves this invariance [21,22]. This implies the exact exponent identity $\nu_\parallel + \zeta_\parallel = 2$, for the special case $\lambda_\parallel = \lambda_\perp$.

B. Generalized Cole-Hopf (CH) transformation

The CH transformation is a useful tool in studying the exact solutions to the one-component ($n = 0$) nonlinear diffusion equation [20]. Here, we generalize this transformation to arbitrary n. Consider a set of $n + 1$ linearly independent $s \times s$ complex matrices $\mathcal{A} = \{A^j, \ j = 0, n\}$. Let the *anticommutator* of two matrices be defined as

$$\{A, B\} = \tfrac{1}{2}(AB + BA). \qquad (2.5)$$

The vector space spanned by $\mathcal{A}$ becomes a *special Jordan algebra* [24] if, for any $(A^i, A^j) \in \mathcal{A}$,

$$\{A^i, A^j\} = \epsilon^{ij}_k A^k \ , \qquad (2.6)$$

with *real* coefficients ϵ^{ij}_k, and $A^k \in \mathcal{A}$ [25]. We will show next that for each such algebra, there is a nonlinear mapping which connects a linear diffusion equation to a set of nonlinear evolution equations similar to (1.5).

Let $W(x,t) = \exp(\lambda_\parallel r_\alpha A^\alpha / 2D)$, where $r_\alpha(x,t)$ are $n+1$ scalar functions. If W satisfies the diffusion equation,

$$\partial_t W = D\partial^2_x W \ , \qquad (2.7)$$

the corresponding equations of motion for r_α are obtained from

$$\partial_t W = \frac{\lambda_\parallel}{2D}\partial_t r_\alpha A^\alpha W, \qquad (2.8)$$

$$\partial^2_x W = \frac{\lambda_\parallel}{2D}\left(\partial^2_x r_\alpha A^\alpha + \frac{\lambda_\parallel}{2D}\partial_x r_\beta \partial_x r_\gamma \{A^\beta, A^\gamma\}\right) W \ . \qquad (2.9)$$

Substituting back in Eq. (2.7), and making use of the relation (2.6), we find

$$\partial_t r_\alpha A^\alpha W = \left(D\partial_x^2 r_\alpha + \epsilon_\alpha^{\beta\gamma} \frac{\lambda_\parallel}{2} \partial_x r_\beta \partial_x r_\gamma \right) A^\alpha W. \quad (2.10)$$

By construction, $\det(W) \neq 0$, and the matrices A^α are linearly independent. Therefore, the scalar functions must satisfy

$$\partial_t r_\alpha = D\partial_x^2 r_\alpha + \frac{\lambda_\parallel}{2} \epsilon_\alpha^{\beta\gamma} \partial_x r_\beta \partial_x r_\gamma \ . \quad (2.11)$$

The relation between Eqs. (1.5) and (2.11) is now easy to establish. First of all, one needs $D_\parallel = D_\perp = D$. If we let $r_0 \equiv r_\parallel$ and $r_i \equiv r_{\perp i}$ $(i = 1, n)$, then the *structure factors* ϵ_k^{ij} must satisfy

$$\begin{aligned} &\epsilon_0^{00} = 1, \\ &\epsilon_0^{ii} = \lambda_\times/\lambda_\parallel \ \ (i = 1, n) \ , \\ &\epsilon_i^{i0} = \epsilon_i^{0i} = \lambda_\perp/\lambda_\parallel \ \ (i = 1, n) \ , \\ &\epsilon_i^{jk} = 0, \ \ \text{otherwise.} \end{aligned} \quad (2.12)$$

One out of the many possible algebras for cases up to $n = 3$ is given in Table III, along with the special conditions when they are applicable. Unfortunately, there are no such algebras for which $\lambda_\perp < 0$, and in all given algebras, $\lambda_\perp = \lambda_\parallel$ is required.

This transformation enables us to solve the *deterministic* equations exactly, for any given initial conditions $r_\alpha(x, 0)$. It is also possible to write the solution to the *stochastic* equation in the form of a path integral. The answer is relatively simple for the case $n = 1$, since one can use a simple algebra $\mathcal{A} = \{1, i\sqrt{-\lambda_\times/\lambda_\parallel}\}$ (for $\lambda_\times < 0$), so that, for

$$W(x,t) = \exp\left(\frac{\lambda_\parallel r_\parallel(x,t) + i\sqrt{-\lambda_\parallel \lambda_\times} r_\perp(x,t)}{2D} \right) \quad (2.13)$$

the linear diffusion equation

$$\partial_t W = D\partial_x^2 W + \mu(x,t) W, \quad (2.14)$$

leads to Eqs. (1.5) with $D_\parallel = D_\perp = D$ and $\lambda_\parallel = \lambda_\perp$. [Here $\mathrm{Re}(\mu) = \lambda_\parallel \eta_\parallel / 2D$ and $\mathrm{Im}(\mu) = \sqrt{-\lambda_\parallel \lambda_\times}\, \eta_\perp / 2D$.] Therefore, the solution to the *stochastic* equation can be written as the path integral

$$W(x,t) = \int_{(0,0)}^{(x,t)} \mathcal{D}x'(\tau) \exp\left\{ -\int_0^t d\tau \left[\frac{\dot{x}'^2}{2D} + \mu(x',\tau) \right] \right\}. \quad (2.15)$$

TABLE III. Jordan algebras suitable for use in the generalized Cole-Hopf transformation for up to $n = 3$. For a given n, the corresponding algebra consists of the matrices $\{A_\alpha, \alpha = 0, n\}$. σ_α (for $\alpha = 1, 2, 3$) are the well-known Pauli matrices; generators of the su(2) algebra together with the 2×2 identity matrix.

Case[a]	A_0	A_1	A_2	A_3
$\lambda_\times > 0$	I	$\sqrt{\lambda_\times/\lambda_\parallel}\sigma_1$	$\sqrt{\lambda_\times/\lambda_\parallel}\sigma_2$	$\sqrt{\lambda_\times/\lambda_\parallel}\sigma_3$
$\lambda_\times < 0$	I	$i\sqrt{\lambda_\times/\lambda_\parallel}\sigma_1$	$i\sqrt{\lambda_\times/\lambda_\parallel}\sigma_2$	$i\sqrt{\lambda_\times/\lambda_\parallel}\sigma_3$

[a]In all cases, $D_\parallel = D_\perp = \nu$ and $\lambda_\perp = \lambda_\parallel$.

Equation (2.15) has been extensively studied in connection with quantum tunneling in a disordered medium [26], with W representing the wave function. In particular, results for the tunneling probability $|W|^2$ suggest $\nu_\parallel = 1/2$ and $z_\parallel = 3$. The transverse fluctuations correspond to the phase in the quantum problem which is not an observable. Hence this mapping does not provide any information on $\nu_\perp$ and $z_\perp$ which are in fact observable in the polymer problem. In the presence of spin-orbit scattering, the tunneling of the electron is described by the evolution of a two-component spinor. The resulting path integral is similar to the above equation, but the impurities μ now include random rotations. The problem is thus similar to the above, with the matrices $\mathcal{A}$ corresponding to generators of the su(2) algebra. This example corresponds to $n = 3$. Discussion of other values of n is beyond the scope of this paper.

C. Fluctuation-dissipation (FD) condition

From the Langevin Eqs. (1.5), we can also construct a Fokker-Planck equation for the time evolution of the joint probability $\mathcal{P}(r_\parallel(x), r_{\perp i}(x))$ for the case of uncorrelated (white) noise as

$$\partial_t \mathcal{P} = \int dx \sum_\alpha \left(\frac{\delta \mathcal{P}}{\delta r_\alpha(x)} \cdot \partial_t r_\alpha + T_\alpha \frac{\delta^2 \mathcal{P}}{\delta r_\alpha^2(x)} \right). \quad (2.16)$$

Since Eqs. (1.5) are not generated from a Hamiltonian, it is not *a priori* clear that the above equation has a stationary solution. Nevertheless, the probability distribution

$$\mathcal{P}_0 = \exp\left(-\int dx \left[\frac{D_\parallel}{2T_\parallel} (\partial_x r_\parallel)^2 + \frac{D_\perp}{2T_\perp} \sum_i (\partial_x r_{\perp i})^2 \right] \right), \quad (2.17)$$

upon substituting in Eq. (2.16), satisfies

$$\frac{1}{\mathcal{P}_0} \frac{\partial \mathcal{P}_0}{\partial t} = -\int dx \left\{ \frac{D_\parallel \lambda_\parallel}{2T_\parallel} (\partial_x^2 r_\parallel)(\partial_x r_\parallel)^2 + \sum_i \left[\frac{D_\parallel \lambda_\times}{2T_\parallel} (\partial_x^2 r_\parallel)(\partial_x r_{\perp i})^2 + \frac{D_\perp \lambda_\perp}{T_\perp} (\partial_x^2 r_{\perp i})(\partial_x r_\parallel)(\partial_x r_{\perp i}) \right] \right\}. \quad (2.18)$$

The first term in the integrand is a complete derivative,

$$(\partial_x^2 r_\parallel)(\partial_x r_\parallel)^2 = \partial_x [\tfrac{1}{3} (\partial_x r_\parallel)^3], \quad (2.19)$$

and gives no contribution to the integral, since boundary terms vanish (only profiles with $\lim_{x \to \pm\infty} \partial_x r_\alpha = 0$ have nonzero probability [27].) The remaining terms can also be combined into a complete derivative,

$$\partial_x [(\partial_x r_\parallel)(\partial_x r_{\perp i})^2] = (\partial_x^2 r_\parallel)(\partial_x r_{\perp i})^2 + 2(\partial_x r_\parallel)(\partial_x r_{\perp i})(\partial_x^2 r_{\perp i}), \quad (2.20)$$

provided that $\lambda_\times D_\parallel T_\perp = \lambda_\perp D_\perp T_\parallel$. Thus for this special choice of parameters, depicted by a starred line in Fig. 2,

the probability distribution of Eq. (2.17) is a stationary solution of the Fokker-Planck equation. If $\mathcal{P}$ converges to this solution, the response functions of the full system are related to this stationary solution through a FDT [21,28]. This implies a nonrenormalization of the "bare" parameters $T_\parallel/D_\parallel$ and $T_\perp/D_\perp$, which appear both in the original equation of motion (1.5) and the full response functions (1.7). Thus the long-time behavior of the correlation functions in Eq. (1.7) can be directly read off from the naive scaling of these ratios, giving $\nu_\parallel = \nu_\perp = 1/2$. For $D_\parallel = D_\perp$ and $T_\parallel = T_\perp$, the stationary distribution is identical to that of the Rouse model. However, when $D_\parallel T_\perp \neq D_\perp T_\parallel$, the average stationary shape will be a ellipsoid with $\langle r_\parallel^2\rangle/\langle r_\perp^2\rangle = D_\perp T_\parallel/D_\parallel T_\perp = \lambda_\times/\lambda_\perp$. This quantity varies continuously along the FDT subspace. The nonspherical shape results in a form birefringence that originates from the nonlinearities.

As we shall see in the following sections, the large-N behavior is controlled by this subspace, at least in the low-field limit. It is therefore possible to determine the nonlinearities $\{\lambda\}$ by macroscopic measurements. In order to do this, consider the situation where a stretching force $\mathbf{f}$ is applied to the two ends of the polymer. This will alter $\mathcal{P}_0$ only by the change

$$\partial_x r_\parallel \mapsto (\partial_x r_\parallel - s f_\parallel),\ \partial_x r_{\perp i} \mapsto (\partial_x r_{\perp i} - s f_{\perp i}).$$

(s is a constant describing the amount of stretching.) This modified distribution describes a rod of length proportional to sN with transverse fluctuations that scale as $\sqrt{N}$. Thus, the polymer behaves as a slender rod, and the nonlinear terms can be obtained by measuring the orientational dependence of the mobility.

III. RENORMALIZATION-GROUP (RG) ANALYSIS

The information on exponents and the dynamic universality class is contained in the $(k,\omega) \to 0$ limit of the noise-averaged correlations in Eq. (1.7), which after Fourier transforming in space and time read

$$\langle r_\alpha(k,\omega) r_\alpha(k',\omega')\rangle = \delta(k+k')\delta(\omega+\omega') \times |k|^{\zeta_\alpha - 1 - 2\nu_\alpha} f\left(\frac{\omega}{|k|^{\zeta_\alpha}}\right). \quad (3.1)$$

Following a change of scale to $x \to bx$, accompanied by $t \to b^\zeta t$ and $r_\alpha \to b^{\nu_\alpha} r_\alpha$, Eqs. (1.5) transform into

$$b^{\nu_\parallel - \zeta}\partial_t r_\parallel = D_\parallel b^{\nu_\parallel - 2}\partial_x^2 r_\parallel + \frac{\lambda_\parallel}{2} b^{2\nu_\parallel - 2}(\partial_x r_\parallel)^2 + \frac{\lambda_\times}{2} b^{2\nu_\perp - 2}\sum_{i=1}^{n}(\partial_x r_{\perp i})^2 + b^{-(1+\zeta)/2}\eta_\parallel(x,t), \quad (3.2a)$$

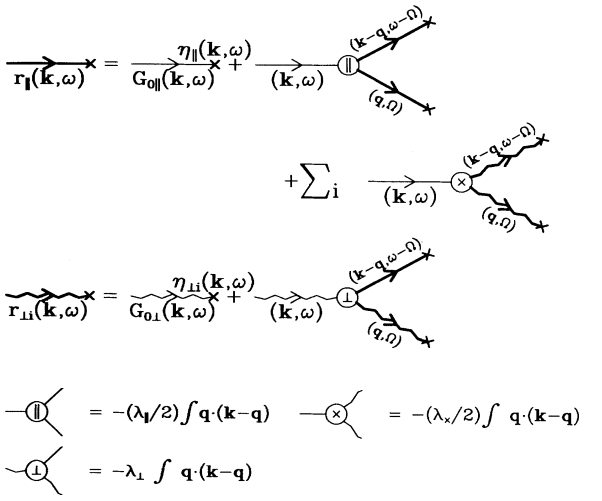

FIG. 3. Diagrammatic representation of the nonlinear integral equations (3.5).

$$b^{\nu_\perp - \zeta}\partial_t r_{\perp i} = D_\perp b^{\nu_\perp - 2}\partial_x^2 r_{\perp i} + \lambda_\perp b^{\nu_\parallel + \nu_\perp - 2}\partial_x r_\parallel \partial_x r_{\perp i} + b^{-(1+\zeta)/2}\eta_{\perp i}(x,t). \quad (3.2b)$$

Equation (1.6) is used to determine the scaling of noise. We conclude that the parameters of the equations transform to

$$\begin{aligned} D_\alpha &\to b^{\zeta-2} D_\alpha, \\ T_\alpha &\to b^{\zeta - 2\nu_\alpha - 1} T_\alpha, \\ \lambda_\parallel &\to b^{\nu_\parallel + \zeta - 2}\lambda_\parallel, \\ \lambda_\perp &\to b^{\nu_\parallel + \zeta - 2}\lambda_\perp, \\ \lambda_\times &\to b^{2\nu_\perp - \nu_\parallel + \zeta - 2}\lambda_\times. \end{aligned} \quad (3.3)$$

When all three nonlinear terms are absent, the equations become scale invariant upon the choice of $\zeta = 2$, $\nu_\parallel = \nu_\perp = 1/2$. However, all three nonlinearity parameters grow under rescaling. They are therefore *relevant* and may change the scaling exponents. For example, when $\lambda_\parallel > 0$, $\lambda_\perp = \lambda_\times = 0$, Eqs. (1.5) decouple and reduce to a KPZ equation (for $r_\parallel$) and n diffusion equations (for $r_{\perp i}$), with the exponents

$$\zeta_\parallel = 3/2,\ \zeta_\perp = 2,\ \nu_\parallel = \nu_\perp = 1/2. \quad (3.4)$$

In order to calculate the exponents in the presence of nonlinearities, we can reorganize Eqs. (1.5) into a form suitable for a perturbative calculation of $\mathbf{r}(k,\omega)$ in powers of the nonlinearities $\{\lambda\}$. Fourier transforming Eqs. (1.5) in space and time, after some rearrangement, yields

$$r_\parallel(k,\omega) \equiv G_\parallel(k,\omega)\eta_\parallel(k,\omega) = G_{0\parallel}(k,\omega)\eta_\parallel(k,\omega) - \frac{\lambda_\parallel}{2}\int\frac{d\Omega}{2\pi}\int^\Lambda \frac{dq}{2\pi} q(k-q) r_\parallel(q,\Omega) r_\parallel(k-q,\omega-\Omega) - \frac{\lambda_\times}{2}\sum_i \int\frac{d\Omega}{2\pi}\int^\Lambda \frac{dq}{2\pi}\, q(k-q)\, r_{\perp i}(q,\Omega) r_{\perp i}(k-q,\omega-\Omega), \quad (3.5a)$$

$$r_{\perp i}(k,\omega) \equiv G_{\perp}(k,\omega)\eta_{\perp i}(k,\omega) = G_{0\perp}(k,\omega)\eta_{\perp i}(k,\omega) - \lambda_{\perp}\int\frac{d\Omega}{2\pi}\int^{\Lambda}\frac{dq}{2\pi}\, q(k-q)\, r_{\perp i}(q,\Omega)r_{\parallel}(k-q,\omega-\Omega). \tag{3.5b}$$

Here, $G_{0\alpha}$'s are bare propagators $(D_\alpha k^2 - i\omega)^{-1}$ in the absence of nonlinearities, and Λ is a suitable short distance cutoff. This set of nonlinear integral equations is indicated diagrammatically in Fig. 3. The averaging is done using the Fourier transform of Eqs. (1.6), which reads

$$\langle \eta_\alpha(k,\omega)\eta_\beta(k',\omega')\rangle = 2T_\alpha\delta_{\alpha,\beta}\delta(k+k')\delta(\omega+\omega'). \tag{3.6}$$

The perturbative expressions for the effective response functions $G_{\parallel}, G_{\perp}$ are represented diagrammatically in Fig. 4. (The combinatorial factor for each diagram is found by counting all possible noise contractions that give rise to it.) Actually, the dimensionless perturbative parameters are of the form $\lambda^2 T/D^3$. Since $G_0(k,0) = 1/Dk^2$, one can define an effective tension $\tilde{D}$ from $G(k,0) = 1/\tilde{D}k^2$. Similarly, an effective spectral density function $\tilde{T}(k,\omega)$ is defined by

$$\langle r^*_\alpha(k,\omega)r_\alpha(k,\omega)\rangle = 2\tilde{T}_\alpha(k,\omega)G_\alpha(k,w)G_\alpha(-k,-w),$$

and calculated perturbatively by the series shown in Fig. 5. Effective vertex functions are similarly computed perturbatively by the series shown in Fig. 6. The corrections to the bare parameters diverge at small loop momenta. We therefore reorganize the summation of these corrections in order to avoid singularities. The RG procedure works as follows: We average noise over a momentum shell $\Lambda e^{-\ell} < |k| < \Lambda$ and find the contribution of this averaging to the parameters, after which we make a change of scale $x \to e^{\ell}x$, $t \to e^{\zeta\ell}t$, $r_{\parallel} \to e^{\nu_{\parallel}\ell}r_{\parallel}$, $r_{\perp i} \to e^{\nu_\perp \ell}r_{\perp i}$. This procedure gives rise to recursion relations for the effective parameters in Eqs. (1.5). The calculations are lengthy and not particularly instructive as a straightforward generalization of those in Ref. [21]. Details of the calculation are given in Appendixes C, D, and E. The resulting recursion relations are

$$\frac{dD_{\parallel}}{d\ell} = D_{\parallel}\left[\zeta - 2 + K_1\frac{\lambda_{\parallel}^2 T_{\parallel}}{4D_{\parallel}^3} + nK_1\frac{\lambda_\perp\lambda_\times T_\perp}{4D_{\parallel}D_\perp^2}\right], \tag{3.7a}$$

$$\frac{dD_\perp}{d\ell} = D_\perp\left[\zeta - 2 + K_1\frac{\lambda_\perp[(\lambda_\times T_\perp/D_\perp) + (\lambda_\perp T_{\parallel}/D_{\parallel})]}{2D_\perp(D_\perp + D_{\parallel})} + K_1\frac{D_\perp - D_{\parallel}}{D_\perp + D_{\parallel}}\frac{\lambda_\perp[(\lambda_\times T_\perp/D_\perp) - (\lambda_\perp T_{\parallel}/D_{\parallel})]}{D_\perp(D_\perp + D_{\parallel})}\right], \tag{3.7b}$$

$$\frac{dT_{\parallel}}{d\ell} = T_{\parallel}\left[\zeta - 2\nu_{\parallel} - 1 + K_1\frac{\lambda_{\parallel}^2 T_{\parallel}}{4D_{\parallel}^3}\right] + nK_1\frac{\lambda_\times^2 T_\perp^2}{4D_\perp^3}, \tag{3.7c}$$

$$\frac{dT_\perp}{d\ell} = T_\perp\left[\zeta - 2\nu_\perp - 1 + K_1\frac{\lambda_\perp^2 T_{\parallel}}{D_\perp D_{\parallel}(D_\perp + D_{\parallel})}\right], \tag{3.7d}$$

$$\frac{d\lambda_{\parallel}}{d\ell} = \lambda_{\parallel}\left[\nu_{\parallel} + \zeta - 2\right], \tag{3.7e}$$

$$\frac{d\lambda_\perp}{d\ell} = \lambda_\perp\left[\nu_{\parallel} + \zeta - 2 - K_1\frac{\lambda_{\parallel} - \lambda_\perp}{(D_\perp + D_{\parallel})^2}[(\lambda_\times T_\perp/D_\perp) - (\lambda_\perp T_{\parallel}/D_{\parallel})]\right], \tag{3.7f}$$

$$\frac{d\lambda_\times}{d\ell} = \lambda_\times\left[2\nu_\perp - \nu_{\parallel} + \zeta - 2 + K_1\frac{\lambda_{\parallel}D_\perp - \lambda_\perp D_{\parallel}}{D_\perp D_{\parallel}(D_\perp + D_{\parallel})}[(\lambda_\times T_\perp/D_\perp) - (\lambda_\perp T_{\parallel}/D_{\parallel})]\right]. \tag{3.7g}$$

Starting from a given set of "bare" parameters, the RG flows are generated by integrating these differential equations, corresponding to a repeated application of an infinitesimal renormalization of the system. The exponents $\zeta(\ell)$ and $\nu_{\parallel}(\ell)$ are chosen such that $D_{\parallel}$ and $\lambda_{\parallel}$ remain scale invariant, i.e.,

$$\frac{dD_{\parallel}}{d\ell} = \frac{d\lambda_{\parallel}}{d\ell} = 0.$$

The exponent $\nu_\perp$ can actually be eliminated from the recursion relations by considering the renormalization of $\lambda_\times T_\perp$ since only this combination appears in the recursion relations. The value of this exponent can later be determined by demanding scale invariance for each of the parameters $\lambda_\times, T_\perp$ separately. This way, the flow of all the parameters is determined, along with the scaling exponents. The RG flows and resulting exponents are indicated in Fig. 2 and Table I, respectively. The resulting flows naturally satisfy the constraints imposed by the nonperturbative results: the subspace of GI is closed under RG, while the FD condition appears as a *fixed line.*

A. Different dynamical exponents

With the above RG procedure it is difficult to address circumstances when the different components have *distinct* dynamical scaling. As long as the "fixed-point equations" are coupled, it is natural to choose $\zeta_{\parallel} = \zeta_\perp$. However, when $\zeta_{\parallel} \neq \zeta_\perp$, the RG flows terminate at a region of parameter space that is not perturbatively accessible.

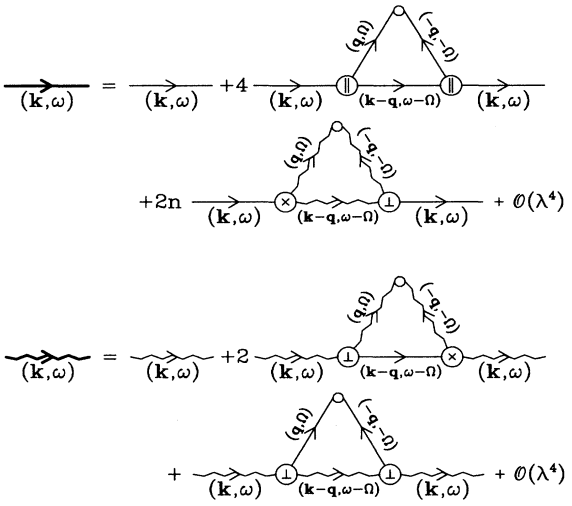

FIG. 4. Leading corrections to the longitudinal and transverse propagators $G_{\|}, G_{\perp}$ in the perturbative expansion of Fig. 3 after averaging over noise.

In order to demonstrate this, let us examine a simpler set of equations,

$$\partial_t h_1 = D_1 \partial_x^2 h_1,$$
$$\partial_t h_2 = D_2 \partial_x^4 h_2.$$

These equations can be solved exactly; the dynamical exponents are $\zeta_1 = 2$, $\zeta_2 = 4$. However, when we rescale them together and choose ζ to keep D_1 fixed, we see that $D_2 \to 0$. As long as the equations are decoupled, one can still recover ζ_2 by examining how D_2 flows to the fixed point. But Eqs. (3.7) involve parameters that diverge at such a fixed point. Since the whole RG treatment is only perturbative, a divergence of any perturbative parameter invalidates its results. A different RG treatment or a self-consistent appoach [29,30] may eliminate such problems and enable a systematic analysis of the whole parameter space. We have investigated such regions numerically in order to determine what kinds of properties one might expect. It is also not clear whether such regions of parameter space are accessible to physical systems.

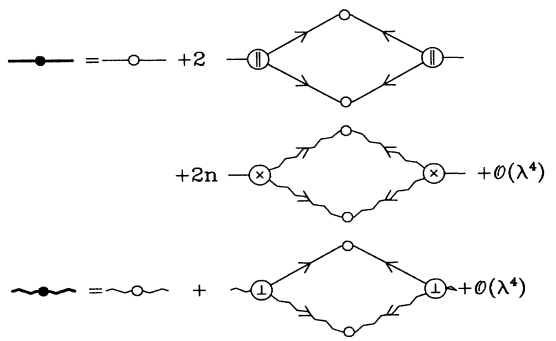

FIG. 5. Leading corrections to the spectral density functions $T_{\|}, T_{\perp}$.

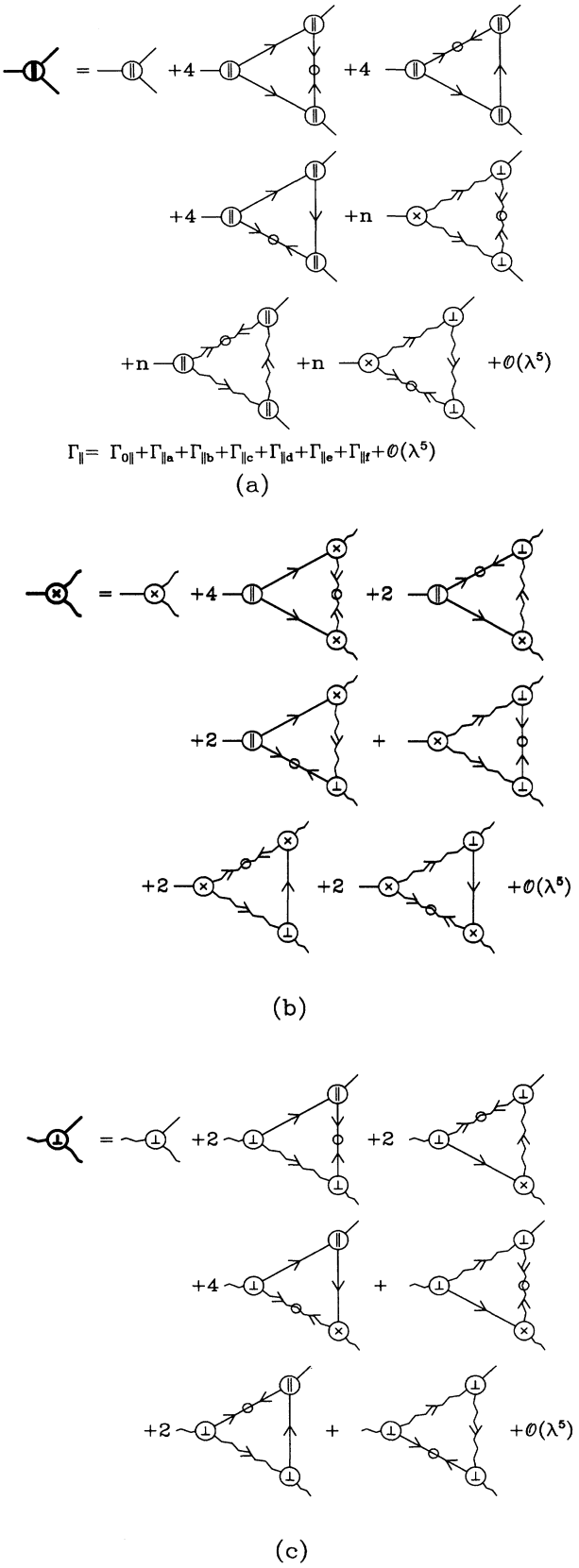

FIG. 6. Leading corrections to the vertex functions (a) $\Gamma_{\|}$, (b) $\Gamma_{\times}$, and (c) $\Gamma_{\perp}$.

B. Fixed points and scaling

The scaling behaviors for the different regions in Fig. 2 are determined by the values of the exponents at the attracting fixed point(s). The results are presented below.

$\lambda_\perp > 0$ *and* $\lambda_\times > 0$. In this quadrant (I), for $n < 4$, the RG flows terminate on the fixed line where FD conditions apply, hence $\nu_\parallel = \nu_\perp = 1/2$. All along this line, the one-loop RG exponent is $\zeta = 3/2$. When $n \geq 4$, the flows indicate that $D_\perp \to 0$, even though $\lambda_\perp$ remains finite and RG is inconclusive. The reason for the breakdown of RG is again the nonperturbative nature of the fixed point. A different scheme is needed when the perturbative parameters diverge [29,30].

$\lambda_\perp < 0$ *and* $\lambda_\times > 0$. The analysis of this region (II) is the most difficult in that the RG flows do not converge upon a finite fixed point *and* $\lambda_\perp \to 0$. Hence we expect $\zeta_\parallel \neq \zeta_\perp$, and a different RG scheme is necessary.

$\lambda_\perp < 0$ *and* $\lambda_\times < 0$. The FD condition again provides a stable fixed line in this quadrant (III), hence $\nu_\parallel = \nu_\perp = 1/2$ and for $n < 4$, the one-loop RG gives $\zeta = 3/2$. For $n \geq 4$, the RG is once again inconclusive.

$\lambda_\perp > 0$ *and* $\lambda_\times < 0$. For $n = 1$, the *projected* RG flows in this quadrant (IV) converge to the point $\lambda_\perp/\lambda_\parallel = 1$ and $\lambda_\times T_\perp D_\parallel/\lambda_\parallel T_\parallel D_\perp = -1$. However, this is not a fixed point, as the noise parameters $T_\parallel$ and $T_\perp$ scale to infinity. Therefore, it is not possible to determine the exponents. Fortunately, the CH transformation is applicable to this point, this suggests $\zeta_\parallel = 3/2$ and $\nu_\parallel = 1/2$.

$\lambda_\times = 0$. In this case the equation for $r_\parallel$ is identical to that of an interface in 1+1 dimensions, and $\nu_\parallel = 1/2$, with $\zeta_\parallel = \zeta_\perp = 3/2$ (since $\lambda_\perp \neq 0$). The fluctuations in $r_\parallel$ act as a strong (multiplicative and correlated) noise on $r_{\perp i}$. The one-loop RG yields an exponent $\nu_\perp = 0.75$ for $\lambda_\perp > 0$, while for $\lambda_\perp < 0$, $\lambda_\perp$ scales to 0 and hence the RG is inconclusive except for implying $\zeta_\perp > \zeta_\parallel$. This result is independent of n.

$\lambda_\perp = 0$. The transverse fluctuations satisfy a simple diffusion equation with $\nu_\perp = 1/2$ and $\zeta_\perp = 2$. Through the term $\lambda_\times(\partial_x r_{\perp i})^2/2$, these fluctuations act as a correlated noise [21] for the longitudinal mode. Since $\zeta_\parallel \neq \zeta_\perp$, the RG is once again inconclusive. Simulations (Table I) indicate different behavior depending on the sign of $\lambda_\times$. This dependence on the sign of $\lambda_\times$ is not too surprising in view of the fundamental difference between behaviors in quadrants II and IV of Fig. 2.

IV. NUMERICAL SIMULATIONS

In this section we discuss the numerical integration of Eqs. (1.5), for various parameter values, to provide a comparison to the RG results. Such simulations have been quite successful in obtaining the scaling properties of the interface growth equation [31]. We use the following discretized equations:

$$
\begin{aligned}
r_\parallel(x,t+dt) &= r_\parallel(x,t) + D_\parallel[r_\parallel(x+1,t) - 2r_\parallel(x,t) + r_\parallel(x-1,t)]dt + \frac{\lambda_\parallel}{8}[r_\parallel(x+1,t) - r_\parallel(x-1,t)]^2 dt \\
&\quad + \frac{\lambda_\times}{8}\sum_i [r_{\perp i}(x+1,t) - r_{\perp i}(x-1,t)]^2 dt + \sqrt{2T_\parallel dt}\,\psi_\parallel(x,t), \\
r_{\perp i}(x,t+dt) &= r_{\perp i}(x,t) + D_\perp[r_{\perp i}(x+1,t) - 2r_{\perp i}(x,t) + r_{\perp i}(x-1,t)]dt \\
&\quad + \frac{\lambda_\perp}{4}[r_{\perp i}(x+1,t) - r_{\perp i}(x-1,t)]^2 dt + \sqrt{2T_\perp dt}\,\psi_{\perp i}(x,t).
\end{aligned}
$$

Here ψ_α are random variables with zero mean and standard deviation of unity, independently chosen for each time step and each site.

Simulations were carried out starting from a point initial state, with periodic boundary conditions. The time step was chosen small enough to avoid short-range instabilities, typically 0.005 to 0.05. At every step, the center-of-mass motion of the polymer was subtracted off, so that $\bar{r}_\alpha(t) = 0$. The scaling exponents were extracted as follows: The mean-squared radii $\langle R_\alpha(t,N)\rangle = \langle (N^{-1}\sum_{j=1}^N [r_\alpha(j,t)]^2)^{1/2}\rangle$ have the dynamical scaling form

$$\langle R_\alpha(t,N)\rangle = N^{\nu_\alpha} f_\alpha^R\left(\frac{N^{\zeta_\alpha}}{t}\right), \tag{4.1}$$

where the scaling functions f_α^R have the asymptotic behaviors

$$\lim_{u\to\infty} f_\alpha^R(u) = A_\alpha u^{-1/z_\alpha} \text{ and } \lim_{u\to 0} f_\alpha^R(u) = B_\alpha, \tag{4.2}$$

with A_α, B_α being constants. Therefore, the large-t, i.e., steady state, behavior of R_α scales as N^{ν_α}, whereas the large-N, small-t behavior grows as t^{1/z_α}. For the steady-state analysis, time averages (instead of ensemble averages, for computational convenience) of $R_\alpha(t,N)$ were calculated for system sizes $N = 16$, 32, 64, 128, and 256 after the system reached steady state. For the dynamic analysis, system width was calculated as a function of time for $N = 10\,000$ to $60\,000$, up to $t = 300$. Numerical integrations were performed for different sets of parameters and for different values of n in Eqs. (1.5), with emphasis on $n = 1$. A sample result for the parameters $D_\parallel = D_\perp = 1$, $\lambda_\parallel = \lambda_\times = \lambda_\perp = 20$, $T_\parallel = T_\perp = 0.01$ is shown in Fig. 7. Not all exponents correspond to the true asymptotic values, due to finite-size effects. The results of the integrations can be summarized as follows.

The exponents for $n = 1$, along with theoretical predictions, are indicated in Table I. Most of the theoretical predictions are supported by these simulations. At the point where GI and FD conditions hold, the exponents match well with the theoretical values. We also see the change in scaling behavior when $\lambda_\times$ or $\lambda_\perp$ approach zero, as predicted by Eqs. (3.7). The values for

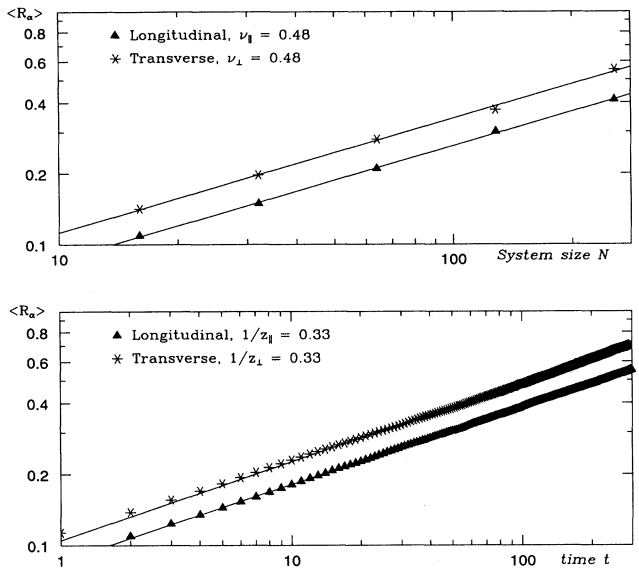

FIG. 7. Top: The longitudinal and transverse sizes of the polymer as a function of its length N. Bottom: Same quantities as a function of time t. The straight lines indicate fits to scaling forms $R \propto N^{\nu}$ and $R \propto t^{1/z}$. Points corresponding to transverse size are shifted up by 30% to avoid data overlap. $\langle R_\alpha \rangle$ and t are in arbitrary units.

swelling exponents for small but positive values of $\lambda_\times$ or $\lambda_\perp$ signify a large crossover regime, with enhanced effective swelling exponents. We expect that the exponents will approach 1/2 at length scales beyond those probed due to computational limitations. This crossover is also evident in the RG equations (3.7), and the flows in Fig. 2. In all cases where the RG method was inconclusive, simulations have either suggested $\zeta_\parallel \neq \zeta_\perp$ or the integration scheme has been unstable in the fully nonlinear regime. A more reliable (and computationally demanding) integration scheme must be used to determine the true asymptotic behavior of these regimes.

It is interesting that even though the nonperturbative properties apply to all n, the perturbative RG breaks down for $n \geq 4$. We therefore integrated the equations for different n at the point where GI and FD conditions were satisfied, in order to search for a potential change in scaling properties. Although the results (Table II) are not completely conclusive, there is strong evidence that $\zeta_\parallel < 3/2 < \zeta_\perp$ for $n > 3$, which is consistent with the RG prediction $D_\perp(\ell)/D_\parallel(\ell) \to 0$. It will be interesting to study the large-n behavior of this system, where it might be possible to obtain a $1/n$ expansion that becomes exact for $n \to \infty$.

V. CONCLUSIONS AND EXTENSIONS

In this work we studied, on the basis of symmetry considerations, a phenomenological model for the relaxation of a polymer drifting due to an external force. In a *local* description nonlinear terms are proposed to describe the dependence of the velocity on the orientation and extension of the polymer. The nonlinearities are relevant, and (for most values of parameters) lead to faster relaxation with a dynamic exponent $z = 3$. The structure factor of the polymer becomes anisotropic as a function of the driving force, and it is even possible for the polymer to undergo a stretching transition. These results could potentially be probed by diffraction and birefringence experiments on sedimenting polymers, or by examining conformations of polymers during electrophoresis. There are other potential applications of the results to defect lines in liquid crystals or flux lines in superconductors. However, our description leaves out a number of potentially important interactions and constraints, such as noise correlations, self-avoidance, and hydrodynamic interactions, reparametrization invariance or arc-length conservation [32]. A number of possible extensions and generalizations are discussed below.

A. Flux lines

A flux line is stretched parallel to the direction of the external magnetic field. The flux line moves due to the Lorentz force in a current. The fluctuations of such a directed line are also described [17] by Eqs. (1.5). In this case $r_\parallel$ denotes fluctuations along the direction of average motion, and $r_{\perp i}$ are the fluctuations in the remaining $n = d - 2$ directions.

B. Drifting manifolds

We can similarly consider the fluctuations of a membrane drifting with an average velocity. In this case two coordinates are needed to describe a point on the membrane. More generally we can consider a d_s-dimensional manifold embedded in a d-dimensional space. (Yet another realization is the coupling of a growing interface to a set of scalar fields.) Except for the change in the dimensionality of the argument $\mathbf{x} = (x_1, \ldots, x_{d_s})$, there is no change in Eqs. (1.5). The only changes in the recursion relations (3.7) come from the rescaling of noise and from angular averages in k space, which appear as overall constants in the correction terms. In the absence of nonlinearities, the Langevin equations are scale invariant with $\zeta_\alpha = 2$, $\nu_\alpha = (2 - d_s)/2$. This swelling exponent is characteristic of tethered manifolds [33]. Thus, for $d_s > 2$, small nonlinearities rescale to zero and are *irrelevant*. In such cases, there is also typically a strong-coupling ($\lambda \neq 0$) region that is not accessible by perturbative methods. For $d_s < 2$, which includes the case extensively discussed, the nonlinearities are relevant, changing the exponents. Perturbation theory breaks down at $d_s = 2$, and more careful analysis is necessary to obtain correct results. Furthermore, the nonperturbative properties discussed, other than GI, no longer hold for $d_s \neq 1$, limiting our knowledge of the problem.

C. Noise correlations

Starting from a microscopic point of view, Eqs. (1.5) are obtained by removing the "fast" degrees of freedom associated with the surrounding fluid. The resulting noise η may acquire long-range correlations in both space and time as a result of this coarse graining. The effects of such correlations have been studied extensively in Ref. [21] for the case $n = 0$. It is straightforward, though somewhat lengthy, to extend the analysis to $n > 0$. Consider noise-noise correlations that asymptotically behave as

$$\langle \eta(k,\omega)\eta(k',\omega')\rangle \sim k^{-2\rho}\omega^{-2\theta}\delta(k+k')\delta(\omega+\omega'). \quad (5.1)$$

The effects of these correlations on scaling exponents depend on the relative signs of nonlinearities, as in the case of uncorrelated noise. For example, for $\theta = 0$ (spatial correlations *only*) it can be shown that when all three nonlinearities have the same sign (quadrant I in Fig. 2), the *renormalized* spectrum is white noise as long as $2\rho < 2\rho_c = 3\nu - 1 = 1/2$. There are no corrections to the scaling exponents calculated without any correlations. The fluctuation-dissipation condition for *uncorrelated noise* suggests an effective "mean-field" noise spectrum characterized by $\rho = \rho_c$. It is precisely for this reason that all correlations decaying more (or equally) rapidly are irrelevant. For $\rho > \rho_c$, the noise spectrum is unrenormalized, except for acquiring a white-noise part, i.e., $T(k) = T_0 + T_\rho k^{-2\rho}$. This results in modified exponents, *exactly* given by the reduced $z = (5-2\rho)/(1+2\rho)$, and the increased $\nu = (1+2\rho)/3$ as in Ref. [21]. On the other hand, when $\lambda_\perp = 0$, the scaling exponents change for $\rho > 0$, as the transverse noise spectrum is unrenormalized (except for acquiring a white-noise part) while the longitudinal correlations are irrelevant for all $\rho \geq 0$. The resulting RG exponents are

$$z_\parallel = (4-4\rho)/(2+4\rho),\ \nu_\parallel = (2+4\rho)/3,$$
$$z_\perp = 4/(1+2\rho),\ \nu_\perp = (1+2\rho)/2.$$

The continuum description naturally breaks down when the chain is fully stretched at $\nu \geq 1$. Temporal correlations, $\theta \neq 0$, complicate the situation by breaking Galilean invariance.

D. Hydrodynamic interactions

In constructing Eqs. (1.5), we only allowed for local effects and ignored the nonlocalities that are the hallmark of hydrodynamics. We shall now demonstrate that (somewhat surprisingly) nonlocal terms are less important at our nonlinear fixed point that at the corresponding Rouse fixed point. One consequence of hydrodynamic interactions is the *back-flow* velocity in Eq. (1.2) that can be added to the evolution equations (1.5). The approximations leading to Eq. (1.2) make this term linear and its main effect is changing the long-wavelength behavior of the bare propagator from $1/q^2$ to $1/q^{3/2}$. Also for the linear Zimm equation to satisfy a fluctuation-dissipation condition, the noise spectrum must be correlated with $2\rho = 1-\nu$ and $\theta = 0$ in Eq. (5.1). Since our nonlinear fixed point also satisfies a fluctuation-dissipation condition, as demonstrated in the previous section, such noise correlations are not relevant, and do not modify the exponents obtained from uncorrelated (local) noise. As for the modified propagator, in d-dimensional space, it acquires an additional term proportional to $q^{d/2}$, with scaling dimension $y_H = \zeta - d/2$. Thus for $d > 3$ the long-range hydrodynamic interactions can be ignored and the scaling exponent $\zeta = 3/2$ is imposed by the nonlinearities. In dimensions $d < 3$ the hydrodynamic interactions are the most relevant, setting $\zeta = d/2$, and the nonlinear terms are irrelevant. In $d = 3$ both terms are equally relevant, and fixed points most likely occur at finite values of both parameters. A more rigorous RG treatment is required to confirm this picture and establish the behavior when both effects are present. In any case it is clear that due to their marginal relevance, the interactions of Eq. (1.2) will not substantially modify previous results. However, once nonlocal terms are included there is no reason to rule out the nonlocal nonlinearity obtained by replacing $\partial_x^2\mathbf{R}$ in Eq. (1.2) by $(\partial_x\mathbf{R})^2$. This nonlinearity also becomes important at the same point when the $\{\lambda\}$ terms become important. It could have important consequences which are left for future studies.

E. Steric interactions

Self-avoidance and entanglement effects are important in low dimensions. The latter are difficult to incorporate and have not been satisfactorily explained. "Soft"-core repulsions can be incorporated in a Hamiltonian and the corresponding equations of motion as an additional term proportional to $b\int dx'\mathcal{V}(\mathbf{r}(x)-\mathbf{r}(x'))$. The relevance of this term is controlled by the scaling dimension $y_{SA} = \zeta - d/2$. This is a rather surprising result, in that the enhanced relaxation actually makes self-avoidance less relevant. If this conclusion is indeed correct, the added constraints should not significantly modify the results in $d = 3$.

ACKNOWLEDGMENTS

We have benefited from discussions with T. Hwa and A. Nadim. This research was supported by the NSF through Grant Nos. DMR-90-01519 and PYI/DMR-89-58061.

APPENDIX A: DERIVATION OF THE EQUATION OF MOTION

In this appendix we present the derivation of Eqs. (1.5) from Eq. (1.4). This is accomplished by a Taylor expansion of $\mathbf{F}$ around $\partial_x R_\alpha = \partial_x^2 R_\alpha = 0$, up to second order and ignoring higher-order gradients. Eliminating terms inconsistent with symmetries, we obtain

$$\partial_t R_\alpha = v_\alpha + Q_\alpha^\beta \partial_x^2 R_\beta + \tfrac{1}{2} T_\alpha^{\beta\gamma} \partial_x R_\beta \partial_x R_\gamma + \text{higher-order terms}, \tag{A1}$$

where v, Q, T are tensors of first, second and third rank, determined only by $\mathbf{e}(x,t)$. Terms proportional to R_α and $\partial_x R_\alpha$ are excluded because of the symmetries $\mathbf{R} \mapsto \mathbf{R} + \mathbf{c}$ and $x \mapsto -x$, respectively. The remaining terms are of higher order in the derivatives. Since the external field $\mathbf{E}$ is the only source of breaking isotropy, it appears in these tensors as

$$\begin{aligned} v_\alpha &= a_1 E_\alpha + (a_2 \delta_\alpha^\beta + a_3 E_\alpha E_\beta)\delta e_\beta + O(||\delta \mathbf{e}||^2), \\ Q_\alpha^\beta &= b_1 \delta_\alpha^\beta + b_2 E_\alpha E_\beta + \mathcal{O}(||\delta \mathbf{e}||), \\ T_\alpha^{\beta\gamma} &= c_1(\delta_\alpha^\beta E_\gamma + \delta_\alpha^\gamma E_\beta) + c_2 \delta_\beta^\gamma E_\alpha + c_3 E_\alpha E_\beta E_\gamma + \mathcal{O}(||\delta \mathbf{e}||). \end{aligned} \tag{A2}$$

Here a_j, b_j, and c_j are constants, and we have neglected (irrelevant) higher-order effects of fluctuations.

The first term in the expansion of v_α is a constant and can be absorbed by defining

$$\mathbf{r}(x,t) = \mathbf{R}(x,t) - a_1 \mathbf{E} t.$$

Choosing the coordinate axes such that $E_\parallel = E$, $E_{\perp i} = 0$, and defining

$$\begin{aligned} D_\parallel &= b_1 + b_2 E^2, \\ D_\perp &= b_1, \\ \lambda_\parallel &= (2c_1 + c_2)E + c_3 E^3, \\ \lambda_\times &= c_2 E, \\ \lambda_\perp &= c_1 E, \\ \eta_\parallel &= (a_2 + a_3 E^2)\delta e_\parallel, \\ \eta_\perp &= a_2 \delta e_\perp, \end{aligned} \tag{A3}$$

we immediately arrive at Eqs. (1.5) and (1.6) with

$$\begin{aligned} 2T_\parallel &= d^{-1}(a_2 + a_3 E^2)^2 \langle ||\delta \dot{\mathbf{e}}||^2 \rangle, \\ 2T_\perp &= d^{-1} a_2^2 \langle ||\delta \mathbf{e}||^2 \rangle. \end{aligned} \tag{A4}$$

APPENDIX B: DERIVATION OF LEADING NONLINEAR TERMS FROM SLENDER-BODY HYDRODYNAMICS

In this appendix we will derive the leading-order *local* nonlinearities in the equation of motion (1.5) in the low Reynolds number limit. In order to do this, consider a rodlike conformation of the polymer with monomer length b_0 where $\partial_x r_\alpha = b_0 t_\alpha$ everywhere on the polymer, so that the elastic (Rouse) force vanishes. If a uniform force $\mathbf{E}$ per monomer acts on this rod, the velocity of the rod can be solved using Kirkwood theory, and the result is (Chap. 8 in Ref. [1])

$$\mathbf{v} = \frac{(-\ln \kappa)}{4\pi \eta_s b_0} \mathbf{E} \cdot [\mathbf{I} + \mathbf{tt}]. \tag{B1}$$

In the above equation, η_s is the solvent viscosity, $\mathbf{I}$ is the identity tensor, $\mathbf{t}$ is the unit tangent vector, and $\kappa = 2b/b_0 N$ is the ratio of the width b to the half length $b_0 N/2$ of the polymer. Direct comparison with Eqs. (A1) and (A2) gives

$$a_1 + \frac{c_2}{2} = C, \; c_1 = C, \; c_3 = 0,$$

where $C = (-\ln \kappa)/4\pi \eta_s b_0$. A more detailed calculation of the force in the more general case of an arbitrarily shaped slender body by Khayat and Cox [11] shows that *nonlocal* contributions to the force, which depend on the whole shape of the polymer rather than the local orientation, are $\mathcal{O}(1/(\ln \kappa)^2)$. Therefore, corrections to Eq. (B1) are small when $N \gg b/b_0$. However, the calculation in [11] assumes that the radius of curvature at every point is $\mathcal{O}(N b_0)$, therefore one may argue that nonlocal corrections are small only if the persistence length is much larger than the polymer width. This analysis does not give the value for a_1, but an approximate expression can be found by using the Rouse model, which is essentially the $\lambda = 0$ limit. In that case, the friction coefficient for a monomer of diameter b_0 is $3\pi \eta_s b_0$, i.e.,

$$\mathbf{v} = \frac{1}{3\pi \eta_s b_0} \mathbf{E},$$

which gives

$$a_1 = \frac{1}{3\pi \eta_s b_0}.$$

Therefore, $a_1 \ll C$ if $|\ln \kappa| \gg 1$. We can now use Eq. (A3) to calculate the nonlinearity parameters

$$\lambda_\parallel = 4(C - a_1/2)E, \; \lambda_\times = 2(C - a_1)E, \; \lambda_\perp = CE.$$

All three nonlinearities are positive in this low-field limit.

APPENDIX C: PROPAGATOR RENORMALIZATION

In this and the following appendix, the details of the RG procedure are given for an arbitrary manifold dimension d_s, as mentioned in Sec. V. (The discussion in Secs. I–IV involves the case $d_s = 1$ only.) We start from the symmetrized versions of the one-loop expressions depicted in Fig. 4. Thus, to leading order in the nonlinearity, the propagators are given as

$$G_{\parallel}(\mathbf{k},\omega) = G_{0\parallel}(\mathbf{k},\omega) + G_{0\parallel}^2(\mathbf{k},\omega)\left\{4\left(-\frac{\lambda_{\parallel}}{2}\right)^2\int^{\Lambda}\frac{d^{d_s}\mathbf{q}}{(2\pi)^{d_s}}\int_{-\infty}^{\infty}\frac{d\Omega}{2\pi}\left(\mathbf{q}+\tfrac{\mathbf{k}}{2}\right)\cdot\left(\mathbf{q}-\tfrac{\mathbf{k}}{2}\right)\ \mathbf{k}\cdot\left(\mathbf{q}+\tfrac{\mathbf{k}}{2}\right)\right.$$
$$\times 2T_{\parallel}G_{0\parallel}\left(\mathbf{q}-\frac{\mathbf{k}}{2},\frac{\omega}{2}-\Omega\right)\left|G_{0\parallel}\left(\mathbf{q}+\frac{\mathbf{k}}{2},\frac{\omega}{2}+\Omega\right)\right|^2$$
$$+2n\left(-\frac{\lambda_{\times}}{2}\right)(-\lambda_{\perp})\int^{\Lambda}\frac{d^{d_s}\mathbf{q}}{(2\pi)^{d_s}}\int_{-\infty}^{\infty}\frac{d\Omega}{2\pi}\left(\mathbf{q}+\tfrac{\mathbf{k}}{2}\right)\cdot\left(\mathbf{q}-\tfrac{\mathbf{k}}{2}\right)\ \mathbf{k}\cdot\left(\mathbf{q}+\tfrac{\mathbf{k}}{2}\right)$$
$$\left.\times 2T_{\perp}G_{0\perp}\left(\mathbf{q}-\frac{\mathbf{k}}{2},\frac{\omega}{2}-\Omega\right)\left|G_{0\perp}\left(\mathbf{q}+\frac{\mathbf{k}}{2},\frac{\omega}{2}+\Omega\right)\right|^2\right\}, \tag{C1a}$$

$$G_{\perp}(\mathbf{k},\omega) = G_{0\perp}(\mathbf{k},\omega) + G_{0\perp}^2(\mathbf{k},\omega)\left\{2\left(-\frac{\lambda_{\times}}{2}\right)(-\lambda_{\perp})\int^{\Lambda}\frac{d^{d_s}\mathbf{q}}{(2\pi)^{d_s}}\right.$$
$$\times\int_{-\infty}^{\infty}\frac{d\Omega}{2\pi}\left(\mathbf{q}+\tfrac{\mathbf{k}}{2}\right)\cdot\left(\mathbf{q}-\tfrac{\mathbf{k}}{2}\right)\ \mathbf{k}\cdot\left(\mathbf{q}+\tfrac{\mathbf{k}}{2}\right)$$
$$\times 2T_{\perp}G_{0\parallel}\left(\mathbf{q}-\frac{\mathbf{k}}{2},\frac{\omega}{2}-\Omega\right)\left|G_{0\perp}\left(\mathbf{q}+\frac{\mathbf{k}}{2},\frac{\omega}{2}+\Omega\right)\right|^2$$
$$+(-\lambda_{\perp})^2\int^{\Lambda}\frac{d^{d_s}\mathbf{q}}{(2\pi)^{d_s}}\int_{-\infty}^{\infty}\frac{d\Omega}{2\pi}\left(\mathbf{q}+\tfrac{\mathbf{k}}{2}\right)\cdot\left(\mathbf{q}-\tfrac{\mathbf{k}}{2}\right)\ \mathbf{k}\cdot\left(\mathbf{q}+\tfrac{\mathbf{k}}{2}\right)$$
$$\left.\times 2T_{\parallel}G_{0\perp}\left(\mathbf{q}-\frac{\mathbf{k}}{2},\frac{\omega}{2}-\Omega\right)\left|G_{0\parallel}\left(\mathbf{q}+\frac{\mathbf{k}}{2},\frac{\omega}{2}+\Omega\right)\right|^2\right\}. \tag{C1b}$$

Since we are interested in the hydrodynamic limit, we focus on the leading order in $(\mathbf{k},\omega)$. Using the bare propagators $G_{0\alpha}(\mathbf{k},\omega) = (D_{\alpha}\mathbf{k}^2 - i\omega)^{-1}$, the $\omega \to 0$ limit can be taken right away, modifying Eq. (C1a) to

$$G_{\parallel}(\mathbf{k}) = G_{0\parallel}(\mathbf{k}) + G_{0\parallel}^2(\mathbf{k})\int^{\Lambda}\frac{d^{d_s}\mathbf{q}}{(2\pi)^{d_s}}\left(\mathbf{q}+\tfrac{\mathbf{k}}{2}\right)\cdot\left(\mathbf{q}-\tfrac{\mathbf{k}}{2}\right)\ \mathbf{k}\cdot\left(\mathbf{q}+\tfrac{\mathbf{k}}{2}\right)\int_{-\infty}^{\infty}\frac{d\Omega}{\pi}$$
$$\times\left\{\frac{\lambda_{\parallel}^2 T_{\parallel}}{\left(D_{\parallel}\left[\mathbf{q}-\frac{\mathbf{k}}{2}\right]^2+i\Omega\right)\left(D_{\parallel}^2\left[\mathbf{q}+\frac{\mathbf{k}}{2}\right]^4+\Omega^2\right)}+\frac{n\lambda_{\times}\lambda_{\perp}T_{\perp}}{\left(D_{\perp}\left[\mathbf{q}-\frac{\mathbf{k}}{2}\right]^2+i\Omega\right)\left(D_{\perp}^2\left[\mathbf{q}+\frac{\mathbf{k}}{2}\right]^4+\Omega^2\right)}\right\}. \tag{C2}$$

Above and from now on, we use $G(\mathbf{k}) \equiv G(\mathbf{k},0)$. After performing the frequency integrals,

$$G_{\parallel}(\mathbf{k}) = G_{0\parallel}(\mathbf{k})\left\{1+\frac{1}{D_{\parallel}k^2}\left(\frac{\lambda_{\parallel}^2T_{\parallel}}{D_{\parallel}^2}+\frac{n\lambda_{\times}\lambda_{\perp}T_{\perp}}{D_{\perp}^2}\right)\int^{\Lambda}\frac{d^{d_s}\mathbf{q}}{(2\pi)^{d_s}}\frac{\left(1-\frac{x^2}{4}\right)\left(x\cos\theta+\frac{x^2}{2}\right)}{\left(1+x\cos\theta+\frac{x^2}{4}\right)2\left(1+\frac{x^2}{4}\right)}\right\}, \tag{C3}$$

where $x = k/q$ and $\mathbf{k}\cdot\mathbf{q} = kq\cos\theta$. We can now expand the integrand in a power series in x, keeping only the leading order since $x \propto k \to 0$. The angular part of the q integration can be readily done using the identities

$$\int^{\Lambda} d^{d_s}\mathbf{q} f(q) = S_{d_s}\int_0^{\Lambda} dq\ q^{d_s-1}f(q),$$
$$\int^{\Lambda} d^{d_s}\mathbf{q}\cos\theta f(q) = 0,$$
$$\int^{\Lambda} d^{d_s}\mathbf{q}\cos^2\theta f(q) = \frac{S_{d_s}}{d_s}\int_0^{\Lambda} dq\ q^{d_s-1}f(q),$$

where S_{d_s} is the surface area of a d_s-dimensional unit sphere. The result is

$$\int^{\Lambda} d^{d_s}\mathbf{q}\ldots = \frac{k^2}{2}\frac{S_{d_s}}{(2\pi)^{d_s}}\int_0^{\Lambda} dq\ q^{d_s-3}\left(\frac{1}{2}-\frac{1}{d_s}\right). \tag{C4}$$

This integral is infrared divergent for $d_s < 2$. The RG procedure is used to overcome this problem. Integrating over the larger momenta in an outer shell $\Lambda(1-\delta\ell) < q < \Lambda$, where $\delta\ell$ is infinitesimal, we obtain

$$G_{0\parallel}^{<}(\mathbf{k}) = G_{0\parallel}(\mathbf{k})\left\{1-\frac{\delta\ell K_{d_s}}{d_s/(2-d_s)}\times\left(\frac{\lambda_{\parallel}^2T_{\parallel}}{4D_{\parallel}^3}+\frac{n\lambda_{\times}\lambda_{\perp}T_{\perp}}{4D_{\parallel}D_{\perp}^2}\right)\right\}, \tag{C5}$$

where $K_{d_s} = S_{d_s}\Lambda^{d_s-2}/(2\pi)^{d_s}$. An effective tension de-

fined through $G_{\parallel}^{<}(\mathbf{k}) = 1/(D_{\parallel}^{<}k^2)$ is now obtained as

$$D_{\parallel}^{<} = D_{\parallel}\left\{1 + \frac{\delta\ell K_{d_s}}{d_s/(2-d_s)}\left(\frac{\lambda_{\parallel}^2 T_{\parallel}}{4D_{\parallel}^3} + \frac{n\lambda_{\times}\lambda_{\perp}T_{\perp}}{4D_{\parallel}D_{\perp}^2}\right)\right\}. \tag{C6}$$

Under a rescaling $k \to (1-\delta\ell)k$, $\omega \to (1-\zeta\delta\ell)\omega$, $r_\alpha \to (1-\nu_\alpha\delta\ell)r_\alpha$, the effective tension $\tilde{D}_{\parallel}$ scales as

$$\tilde{D}_{\parallel} = D_{\parallel} + \frac{dD_{\parallel}}{d\ell}\delta\ell = D_{\parallel}^{<}[1 + \delta\ell(\zeta - 2)].$$

Combining the two, we find the differential recursion relation for $D_{\parallel}$,

$$\frac{dD_{\parallel}}{d\ell} = D_{\parallel}\left\{\zeta - 2 + \frac{K_{d_s}}{d_s/(2-d_s)} \times \left(\frac{\lambda_{\parallel}^2 T_{\parallel}}{4D_{\parallel}^3} + \frac{n\lambda_{\times}\lambda_{\perp}T_{\perp}}{4D_{\parallel}D_{\perp}^2}\right)\right\}. \tag{C7}$$

For $d_s = 1$, this reduces to the form given in Eqs. (3.7).

Very similar steps are followed for the transverse propagator. Starting from Eq. (C1b), we have

$$G_{\perp}(\mathbf{k}) = G_{0\perp}(\mathbf{k}) + G_{0\perp}^2(\mathbf{k})\int^{\Lambda}\frac{d^{d_s}\mathbf{q}}{(2\pi)^{d_s}}\left(\mathbf{q}+\tfrac{\mathbf{k}}{2}\right)\cdot\left(\mathbf{q}-\tfrac{\mathbf{k}}{2}\right)\ \mathbf{k}\cdot\left(\mathbf{q}+\tfrac{\mathbf{k}}{2}\right)\int_{-\infty}^{\infty}\frac{d\Omega}{\pi} \times\left\{\frac{\lambda_{\times}\lambda_{\perp}T_{\perp}}{\left(D_{\parallel}\left[\mathbf{q}-\frac{\mathbf{k}}{2}\right]^2 + i\Omega\right)\left(D_{\perp}^2\left[\mathbf{q}+\frac{\mathbf{k}}{2}\right]^4 + \Omega^2\right)} + \frac{\lambda_{\perp}^2 T_{\parallel}}{\left(D_{\perp}\left[\mathbf{q}-\frac{\mathbf{k}}{2}\right]^2 + i\Omega\right)\left(D_{\parallel}^2\left[\mathbf{q}+\frac{\mathbf{k}}{2}\right]^4 + \Omega^2\right)}\right\}. \tag{C8}$$

The frequency integrals are very similar, and upon performing them, we arrive at

$$G_{\perp}(\mathbf{k}) = G_{0\perp}(\mathbf{k})\left\{1 + \frac{1}{D_{\perp}k^2}\int^{\Lambda}\frac{d^{d_s}\mathbf{q}}{(2\pi)^{d_s}} \times\left[\lambda_{\times}\lambda_{\perp}T_{\perp}\frac{\left(1-\frac{x^2}{4}\right)\left(x\cos\theta+\frac{x^2}{2}\right)}{D_{\perp}\left(1+x\cos\theta+\frac{x^2}{4}\right)\left[(D_{\perp}+D_{\parallel})\left(1+\frac{x^2}{4}\right)+(D_{\perp}-D_{\parallel})x\cos\theta\right]} + \lambda_{\perp}^2 T_{\parallel}\frac{\left(1-\frac{x^2}{4}\right)\left(x\cos\theta+\frac{x^2}{2}\right)}{D_{\parallel}\left(1+x\cos\theta+\frac{x^2}{4}\right)\left[(D_{\parallel}+D_{\perp})\left(1+\frac{x^2}{4}\right)+(D_{\parallel}-D_{\perp})x\cos\theta\right]}\right]\right\}. \tag{C9}$$

Following similar steps as with $D_{\parallel}$, the final result, after some rearrangement, becomes

$$\frac{dD_{\perp}}{d\ell} = D_{\perp}\left\{\zeta - 2 + K_{d_s}\left[\frac{\lambda_{\perp}\left[(\lambda_{\times}T_{\perp}/D_{\perp}) + (\lambda_{\perp}T_{\parallel}/D_{\parallel})\right]}{2D_{\perp}(D_{\perp}+D_{\parallel})}\left(\frac{2-d_s}{d_s}\right) + \frac{(D_{\perp}-D_{\parallel})}{(D_{\perp}+D_{\parallel})}\frac{\lambda_{\perp}\left[(\lambda_{\times}T_{\perp}/D_{\perp}) - (\lambda_{\perp}T_{\parallel}/D_{\parallel})\right]}{D_{\perp}(D_{\perp}+D_{\parallel})}\left(\frac{1}{d_s}\right)\right]\right\}. \tag{C10}$$

APPENDIX D: SPECTRAL DENSITY-FUNCTION RENORMALIZATION

Steps very similar to Appendix C are followed in order to determine the renormalization of the spectral density function. We can take the $(\mathbf{k},\omega) \to 0$ right away to arrive at

$$2T_{\parallel}^{<} = 2T_{\parallel} + 2\left(-\frac{\lambda_{\parallel}}{2}\right)^2\int^{>}\frac{d^{d_s}\mathbf{q}}{(2\pi)^{d_s}}\int_{-\infty}^{+\infty}\frac{d\Omega}{(2\pi)}\ \mathbf{q}\cdot\mathbf{q}\ \mathbf{q}\cdot\mathbf{q}\left(\frac{(2T_{\parallel})^2}{(D_{\parallel}^2q^4+\Omega^2)^2}\right) + 2n\left(-\frac{\lambda_{\times}}{2}\right)^2\int^{>}\frac{d^{d_s}\mathbf{q}}{(2\pi)^{d_s}}\int_{-\infty}^{+\infty}\frac{d\Omega}{(2\pi)}\ \mathbf{q}\cdot\mathbf{q}\ \mathbf{q}\cdot\mathbf{q}\left(\frac{(2T_{\perp})^2}{(D_{\perp}^2q^4+\Omega^2)^2}\right), \tag{D1}$$

$$2T_{\perp}^{<} = 2T_{\perp} + 2(-\lambda_{\perp})^2\int^{>}\frac{d^{d_s}\mathbf{q}}{(2\pi)^{d_s}}\int_{-\infty}^{+\infty}\frac{d\Omega}{(2\pi)}\ \mathbf{q}\cdot\mathbf{q}\ \mathbf{q}\cdot\mathbf{q}\left(\frac{(2T_{\parallel})(2T_{\perp})}{(D_{\parallel}^2q^4+\Omega^2)(D_{\perp}^2q^4+\Omega^2)}\right). \tag{D2}$$

Upon performing the rescaling and arranging the terms as usual, we obtain

$$\frac{dT_{\|}}{d\ell} = T_{\|}\left\{\zeta - 2\nu_{\|} - d_s + K_{d_s}\frac{\lambda_{\|}^2 T_{\|}}{4D_{\|}^3}\right\} + nK_1\frac{\lambda_{\times}^2 T_{\perp}^2}{4D_{\perp}^3}, \tag{D3}$$

$$\frac{dT_{\perp}}{d\ell} = T_{\perp}\left\{\zeta - 2\nu_{\perp} - d_s + K_{d_s}\frac{\lambda_{\perp}^2 T_{\|}}{D_{\|}D_{\perp}(D_{\|}+D_{\perp})}\right\}. \tag{D4}$$

APPENDIX E: VERTEX RENORMALIZATION

First, we calculate the effective three-point vertex functions $\Gamma_{\|}$, $\Gamma_{\times}$, and $\Gamma_{\perp}$ in the $\omega \to 0$ limit. Let $\hat{k}_i \equiv (\mathbf{k}_i, \omega_i)$. All the diagrams up to one-loop order are shown in Fig. 6. After averaging over shell momenta, the first correction term for $\Gamma_{\|}$ is

$$\begin{aligned}\Gamma_{\|a}^{<}\left(\hat{k}_1; \frac{\hat{k}_1}{2}+\hat{k}_2\,, x\frac{\hat{k}_1}{2}-\hat{k}_2\right) &= \Gamma_{0\|}\left(\hat{k}_1; \frac{\hat{k}_1}{2}+\hat{k}_2, \frac{\hat{k}_1}{2}-\hat{k}_2\right)\frac{\lambda_{\|}^2}{\left(\frac{\mathbf{k}_1}{2}+\mathbf{k}_2\right)\cdot\left(\frac{\mathbf{k}_1}{2}-\mathbf{k}_2\right)}\int^{>}\frac{d^{d_s}\mathbf{q}}{(2\pi)^{d_s}} \\ &\times\int_{-\infty}^{+\infty}\frac{d\Omega}{(2\pi)}\left(\mathbf{q}+\frac{\mathbf{k}_1}{2}\right)\cdot\left(\mathbf{q}-\frac{\mathbf{k}_1}{2}\right)\left(\frac{\mathbf{k}_1}{2}+\mathbf{k}_2\right)\cdot(\mathbf{q}-\mathbf{k}_2)\left(\frac{\mathbf{k}_1}{2}-\mathbf{k}_2\right)\cdot(\mathbf{q}-\mathbf{k}_2) \\ &\times 2T_{\|}G_{0\|}\left(\frac{\mathbf{k}_1}{2}+\mathbf{q},\Omega\right)G_{0\|}\left(\frac{\mathbf{k}_1}{2}-\mathbf{q},-\Omega\right)\left|G_{0\|}(\mathbf{q}-\mathbf{k}_2,\Omega)\right|^2,\end{aligned} \tag{E1}$$

where $\Gamma_{0\|}(\hat{k}_a+\hat{k}_b;\hat{k}_a,\hat{k}_b) \equiv -(\lambda_{\|}/2)\mathbf{k}_a\cdot\mathbf{k}_b G_{0\|}(\hat{k}_a)G_{0\|}(\hat{k}_b)$ is the bare vertex function. It is enough to consider only the leading term in the propagators, which simplifies the evaluation. Upon performing the frequency integral, this equation simplifies to

$$\Gamma_{\|a}^{<} = \Gamma_{0\|}\frac{\lambda_{\|}^2 T_{\|}}{2D_{\|}^3}\int^{>}\frac{d^{d_s}\mathbf{q}}{(2\pi)^{d_s}}q^{-2}\frac{\frac{x^2}{4}\cos^2\theta_1 - y^2\cos^2\theta_2}{\frac{x^2}{4}-y^2}, \tag{E2}$$

where $x = k_1/q$, $y = k_2/q$, $\mathbf{k}_1\cdot\mathbf{q} = k_1 q\cos\theta_1$, $\mathbf{k}_2\cdot\mathbf{q} = k_2 q\cos\theta_2$. The spherical part of the integral is now easily computed to give

$$\Gamma_{\|a}^{<} = \delta\ell\Gamma_{0\|}\left(\frac{K_{d_s}}{d_s}\right)\frac{\lambda_{\|}^2 T_{\|}}{2D_{\|}^3}. \tag{E3}$$

Other correction terms are computed similarly. For example,

$$\begin{aligned}\Gamma_{\|b}^{<}\left(\hat{k}_1; \frac{\hat{k}_1}{2}+\hat{k}_2, \frac{\hat{k}_1}{2}-\hat{k}_2\right) &= \Gamma_{0\|}\left(\hat{k}_1; \frac{\hat{k}_1}{2}+\hat{k}_2, \frac{\hat{k}_1}{2}-\hat{k}_2\right)\frac{\lambda_{\|}^2}{\left(\frac{\mathbf{k}_1}{2}+\mathbf{k}_2\right)\cdot\left(\frac{\mathbf{k}_1}{2}-\mathbf{k}_2\right)}\int^{>}\frac{d^{d_s}\mathbf{q}}{(2\pi)^{d_s}} \\ &\times\int_{-\infty}^{+\infty}\frac{d\Omega}{(2\pi)}\left(\mathbf{q}+\frac{\mathbf{k}_1}{2}\right)\cdot\left(\frac{\mathbf{k}_1}{2}-\mathbf{q}\right)\left(\frac{\mathbf{k}_1}{2}+\mathbf{k}_2\right)\cdot\left(\mathbf{q}+\frac{\mathbf{k}_1}{2}\right)\left(\frac{\mathbf{k}_1}{2}-\mathbf{k}_2\right)\cdot(\mathbf{q}-\mathbf{k}_2) \\ &\times 2T_{\|}G_{0\|}\left(\frac{\mathbf{k}_1}{2}-\mathbf{q},-\Omega\right)G_{0\|}\left(\mathbf{k}_2-\mathbf{q},-\Omega\right)\left|G_{0\|}\left(\mathbf{q}+\frac{\mathbf{k}_1}{2},\Omega\right)\right|^2,\end{aligned} \tag{E4}$$

which gives

$$\Gamma_{\|b}^{<} = -\delta\ell\Gamma_{0\|}\left(\frac{K_{d_s}}{d_s}\right)\frac{\lambda_{\|}^2 T_{\|}}{4D_{\|}^3}. \tag{E5}$$

In the limit $k_1, k_2 \to 0$, $\Gamma_{\|b}^{<} = \Gamma_{\|c}^{<}$. Therefore, the sum of the contributions from the three diagrams adds up to zero. The remaining three diagrams are almost identical to the first three and they contribute

$$\begin{aligned}\Gamma_{\|d}^{<} &= \delta\ell\Gamma_{0\|}n\left(\frac{K_{d_s}}{d_s}\right)\frac{2(\lambda_{\times}/\lambda_{\|})\lambda_{\perp}^2 T_{\perp}}{D_{\perp}^3}, \\ \Gamma_{\|e}^{<} &= \Gamma_{\|f}^{<} = -\delta\ell\Gamma_{0\|}n\left(\frac{K_{d_s}}{d_s}\right)\frac{(\lambda_{\times}/\lambda_{\|})\lambda_{\perp}^2 T_{\perp}}{D_{\perp}^3},\end{aligned} \tag{E6}$$

also adding up to zero. Thus, to this order, $\Gamma_{\|}$ does not have any corrections due to renormalization, giving the recursion relation

$$\frac{d\lambda_{\|}}{d\ell} = \lambda_{\|}(\zeta + \nu_{\|} - 2). \tag{E7}$$

For the calculation of the corrections to $\Gamma_{\times}$ and $\Gamma_{\perp}$, it is useful to observe the simple rules that will give us the correct result by inspection of diagrams, rather than doing the very similar and lengthy calculation over again. First, it is clear that leading-order terms are sufficient for the propagators. This makes it easy to evaluate frequency integrals. Also, the momentum shell integral always gives the contribution $\delta\ell K_{d_s}/d_s$. An important rule

determines the overall sign of each contribution. Diagrams of type $\Gamma_{\|a}$, where the noise contraction is adjacent to both outgoing propagators, have a positive overall sign whereas diagrams where the noise contraction joins the incoming propagator to an outgoing one are negative. These set of rules simplify the task of calculating vertex corrections to evaluating simple frequency integrals, and yield the final results

$$\Gamma^{<}_{\times} = \Gamma_{0\times}\left\{1+\delta\ell\left(\frac{K_{d_s}}{d_s}\right)\left[\frac{\lambda_{\|}\lambda_{\times}T_{\perp}}{D_{\|}D_{\perp}(D_{\|}+D_{\perp})}-\frac{\lambda_{\|}\lambda_{\perp}T_{\|}}{D_{\|}^2(D_{\|}+D_{\perp})}+\frac{\lambda_{\perp}^2T_{\|}}{D_{\|}D_{\perp}(D_{\|}+D_{\perp})}-\frac{\lambda_{\perp}\lambda_{\times}T_{\perp}}{D_{\perp}^2(D_{\|}+D_{\perp})}\right]\right\}, \tag{E8}$$

$$\Gamma^{<}_{\perp} = \Gamma_{0\perp}\left\{1+\delta\ell\left(\frac{K_{d_s}}{d_s}\right)\left[\frac{\lambda_{\|}\lambda_{\perp}T_{\|}(3D_{\|}+D_{\perp})}{2D_{\|}^2(D_{\|}+D_{\perp})^2}-\frac{\lambda_{\perp}\lambda_{\times}T_{\perp}}{2D_{\perp}^2(D_{\|}+D_{\perp})}-\frac{\lambda_{\|}\lambda_{\times}T_{\perp}}{D_{\perp}(D_{\|}+D_{\perp})^2}\right.\right.$$
$$\left.\left.+\frac{\lambda_{\perp}\lambda_{\times}T_{\perp}(3D_{\perp}+D_{\|})}{2D_{\perp}^2(D_{\|}+D_{\perp})^2}-\frac{\lambda_{\|}\lambda_{\perp}T_{\|}}{2D_{\|}^2(D_{\|}+D_{\perp})}-\frac{\lambda_{\perp}^2T_{\|}}{4D_{\|}(D_{\|}+D_{\perp})^2}\right]\right\}. \tag{E9}$$

After rescaling and rearranging terms, these give rise to the recursion relations given in Eqs. (3.7), with the substitution of K_{d_s}/d_s for K_1 in the d_s-dimensional case.

[1] For a recent extensive review on polymer dynamics, see M. Doi and S.F. Edwards, *Theory of Polymer Dynamics* (Oxford University Press, New York, 1986).

[2] P.G. de Gennes, *Scaling Concepts in Polymer Physics* (Cornell University Press, New York, 1979).

[3] R.B. Bird, *Dynamics of Polymeric Liquids* (Wiley, New York, 1987), Vols. 1 and 2.

[4] P.E. Rouse, J. Chem. Phys. **21**, 1272 (1953).

[5] J. Kirkwood and J. Risemann, J. Chem. Phys. **16**, 565 (1948).

[6] B.H. Zimm, J. Chem. Phys. **24**, 269 (1956).

[7] C.J. Farrell, A. Keller, M.J. Miles, and D.P. Pope, Polymer **21**, 1292 (1980); M. Adam and M. Delsanti, Macromolecules **10**, 1229 (1977); G. Meyehoff, Z. Phys. Chem. **4**, 335 (1955); R. Mukherjea and P. Rempp, J. Chim. Phys. **56**, 94 (1959); Y. Tsunashima, N. Nemoto, and M. Kurata, Macromolecules **16**, 584, 1184 (1983).

[8] A. Peterlin, Pure Appl. Chem. **12**, 563 (1966); Adv. Macromol. Chem. **1**, 225 (1968); G.B. Thurston and A. Peterlin, J. Chem. Phys. **46**, 4881 (1967).

[9] P.G. de Gennes, J. Chem. Phys. **60**, 5030 (1974).

[10] For a recent overview on electrophoresis, see J.W. Jorgenson, in *New Directions in Electrophoretic Methods*, ACS Symposium Series No. 335 (American Chemical Society, Washington, DC, 1987).

[11] See, e.g., R.E. Khayat and R.G. Cox, J. Fluid. Mech. **209**, 435 (1989), and references inside.

[12] For the given examples, the Reynolds number is Re $\approx 0.005y$. Therefore, there is a velocity range where the dynamical effects are important *and* low-Reynolds-number hydrodynamics is applicable. However, the derivation of Eqs. (1.5) is solely based on symmetry arguments and not limited to the low-Reynolds-number regime.

[13] M. Kardar, in *Disorder and Fracture*, edited by J.C. Charmet, S. Roux, and E. Guyon (Plenum, New York, 1990); T. Hwa and M. Kardar, Phys. Rev. A **45**, 7002 (1992).

[14] Nontrivial correlations or non-Gaussian distributions of the noise, which may potentially alter the scaling behavior [21,34], require a more general treatment and are not considered here.

[15] M. Kardar, G. Parisi, and Y.-C. Zhang, Phys. Rev. Lett. **56**, 889 (1986).

[16] A.-L. Barabasi, Phys. Rev. A **46**, R2977 (1992).

[17] D. Ertaş and M. Kardar, Phys. Rev. Lett. **69**, 929 (1992).

[18] T. Hwa, Phys. Rev. Lett. **69**, 1552 (1992).

[19] D. Wolf, Phys. Rev. Lett. **67**, 1783 (1991).

[20] J.M. Burgers, *The Nonlinear Diffusion Equation* (Riedel, Boston, 1974).

[21] E. Medina, T. Hwa, M. Kardar, and Y.-C. Zhang, Phys. Rev. A **39**, 3053 (1989).

[22] D. Forster, D.R. Nelson, and M.J. Stephen, Phys. Rev. A **16**, 732 (1977).

[23] It is interesting to note that such coupling to a diffusive field leads to a larger exponent. A number of recent experiments, from immiscible displacement in porous media [35,36] to the evolution of bacterial colonies [37] observe interfaces in 1+1 dimensions with a roughness exponent near 0.8. Various other fields (e.g., fluid pressure, nutrient concentration) are certainly present in such experiments. The given example indicates that coupling to such fields may indeed lead to larger roughness exponents [38].

[24] See, e.g., H. Hanche-Olsen, *Jordan Operator Algebras*, Monographs and Studies in Mathematics Vol. 21 (Pitman, New York, 1984).

[25] Throughout this section, repeated indices are summed over.

[26] E. Medina, M. Kardar, Y. Shapir, and X.-R. Wang, Phys. Rev. Lett. **62**, 941 (1989); E. Medina and M. Kardar, Phys. Rev. B **46**, 9984 (1992).

[27] Similar manipulations for the KPZ equation have been discussed by Y.-C. Zhang, unpublished and private communications.

[28] U. Deker and F. Haake, Phys. Rev. A **11**, 2043 (1975).

[29] M. Schwartz and S.F. Edwards, Europhys. Lett. **20**, 301 (1992).

[30] J.P. Bouchaud and M.E. Cates, Phys. Rev. E **47**, R1455 (1993).

[31] J.G. Amar and F. Family, Phys. Rev. A **45**, 5378 (1992); B. Grossman, H. Guo, and M. Grant, Phys. Rev. A **43**, 1727 (1991).

[32] R.E. Goldstein and D.M. Petrich, Phys. Rev. Lett. **67**, 3203 (1991); A. Moritan, F. Toigo, J. Koplik, and J.R. Banavar, Phys. Rev. Lett. **69**, 3193 (1992).

[33] M. Kardar and D.R. Nelson, Phys. Rev. Lett. **58**, 2774 (1987); Phys. Rev. A **36**, 4020 (1987).
[34] Y.-C. Zhang, J. Phys. (Paris) **51**, 2129 (1990).
[35] M.A. Rubio, C.A. Edwards, A. Dougherty, and J.P Gollub, Phys. Rev. Lett. **63**, 1685 (1989).
[36] V.K. Horváth, F. Family, and T. Vicsek, Phys. Rev. Lett. **67**, 3207 (1991).
[37] T. Vicsek, M. Cserzö, and V.K. Horváth, Physica A **167**, 315 (1990).
[38] For other possible explanations, see Ref. [34]; D. Kessler, H. Levine, and Y. Tu, Phys. Rev. A **43**, 4551 (1991).